

Approximate Bayesian inference for spatial flood frequency analysis

Árni V. Johannesson,¹ Birgir Hrafnkelsson,^{1*} Raphaël Huser,²
Haakon Bakka², Stefan Siegert³

¹University of Iceland,

²King Abdullah University of Science and Technology

³University of Exeter

Abstract

Extreme floods cause casualties, widespread property damage, and damage to vital civil infrastructure. Predictions of extreme floods within gauged and ungauged catchments is crucial to mitigate these disasters. In this paper, a Bayesian framework is proposed for predicting extreme floods using the generalized extreme-value (GEV) distribution. The methodological challenges consist of choosing a suitable parametrization for the GEV distribution when multiple covariates and/or latent spatial effects are involved, balancing model complexity and parsimony using an appropriate model selection procedure, and making inference based on a reliable and computationally efficient approach. Our proposed framework is based on a latent Gaussian model, with a novel multivariate link function for the location, scale and shape parameters of the GEV distribution. This link function is designed to separate the interpretation of the parameters at the latent level and to avoid unreasonable estimates of the shape parameter. Structured additive regression models are proposed for the three parameters at the latent level. Each of these regression models contains fixed linear effects for catchment descriptors, e.g., catchment area and average annual rainfall. Spatial model components are added to the two first latent regression models, to model the residual spatial structure unexplained by the catchment descriptors. To achieve computational efficiency for large datasets with these richly parametrized models, we exploit a Gaussian-based approximation to the posterior density. This approximation relies on site-wise estimates, but, contrary to typical plug-in approaches, the uncertainty in these initial estimates is properly propagated through to the final posterior computations. This two-step inference procedure is an approximation to a full Bayesian inference approach for hierarchical models. We applied the proposed modeling and inference framework to annual peak river flow data from 554 catchments across the United Kingdom. The framework performed well in terms of flood predictions for ungauged catchments and the results show that the spatial model components for the transformed location and scale parameters are both important and neither should be ignored.

1 Introduction

Flood predictions are of great importance for the design, management, operation, and protection of vital infrastructure. To aid flood predictions, gauging stations have been built to observe

and monitor streams, wells, lakes, canals and reservoirs. Flood predictions are typically based on analyses of past observed extremes, and they usually rely on fitting statistical models for extreme floods within gauged catchments. Predictions for ungauged catchments are made possible by using appropriate covariates whose coefficients are learned from gauged catchments, and sometimes also by exploiting spatial correlation across catchments using suitable geostatistical models.

One of the first approaches in flood frequency analysis was the index flood method introduced in Dalrymple (1960). The index flood method is a statistical method that was designed to handle cases where little or no site-specific information is available, by borrowing strength from similar catchments. The index flood method consists of two steps: Regionalization, which identifies geographically and climatologically similar regions, and specification of a regional standardized flood frequency curve for the T -year return level. Various developments have been made to improve the index flood method (Hosking et al., 1985; GREHYS, 1996), and various Bayesian methods have been introduced (Cunnane and Nash, 1974; Rosbjerg and Madsen, 1995; Kuczera, 1999; Martins and Stedinger, 2000). In the United Kingdom (UK), the analysis of floods is commonly tackled with the pooling group method (Robson and Reed, 1999; Kjeldsen and Jones, 2009b), which is a combination of (i) the index flood method based on the use of L -moments (Hosking and Wallis, 2005); and (ii) the region of influence (ROI) approach (Burn, 1990). Further related statistical approaches for the modeling, prediction, and uncertainty assessment of annual peak flow data within gauged and ungauged catchments were proposed by, e.g., Kjeldsen and Jones (2006), Kjeldsen and Jones (2009a), Kjeldsen (2010), and Kjeldsen et al. (2017). More recently, Thorarinsdottir et al. (2018) analyzed annual maximum floods from 203 streamflow stations in Norway based on a Bayesian latent Gaussian model (LGM) with a generalized extreme-value (GEV) distribution at the data level, which is motivated by Extreme-Value Theory (see, e.g., Davison et al. (2012) and Davison and Huser (2015)). They used a multivariate link function specified by identity links for the location and shape parameters and a logarithmic link for the scale parameter. Their model is fairly simple in the sense that it does not contain any spatially correlated random effects (a priori), and inference is performed by drawing samples from the posterior distribution using a Markov chain Monte Carlo (MCMC) algorithm. More complex Bayesian models with spatially correlated random effects were considered by Huerta and Sansó (2007), Davison et al. (2012), Geirsson et al. (2015a) and Dyrddal et al. (2015) in studies of extreme ozone concentrations and/or precipitation (see the details therein) but the datasets in these papers were limited to 19, 36, 40 and 59 stations only, respectively; see also Hrafnkelsson et al. (2012), who used a similar approach for modeling annual minimum and maximum temperatures observed at 72 stations in Iceland. In a similar framework, Sang and Gelfand (2009) modeled extreme precipitation observed on a large regular grid with 1078 grid cells by taking advantage of conditional autoregressive (CAR) priors for the location and scale parameters, along with an additional temporal term for the location parameter, and assuming a constant shape parameter. Sang and Gelfand (2010) then relaxed the conditional independence assumption by using a Gaussian dependence structure at the data level. In the same vein, Cooley and Sain (2010) and Jalbert et al. (2017) modeled extreme precipitation data arising from climate model outputs over large grids, by exploiting their gridded structure using intrinsic Gaussian Markov random field (iGMRF) priors at the latent level of the LGM.

In this paper we propose a novel statistical model for annual peak flow data from 554 catchments across the UK that efficiently exploits spatial information about the catchments. Similarly to Huerta and Sansó (2007), Sang and Gelfand (2009, 2010), Davison et al. (2012), Hrafnkelsson et al. (2012), Dyrddal et al. (2015), Geirsson et al. (2015a), Jalbert et al. (2017) and Thorarinsdottir et al. (2018), our proposed model is an LGM that assumes a GEV distribution at the data level with site-specific location, scale and shape parameters, but its detailed hierarchical

structure and our inference procedure have crucial differences that make it more attractive and amenable to complex and large datasets. Moreover, contrary to Sang and Gelfand (2009, 2010), Cooley and Sain (2010) and Jalbert et al. (2017), the data in our application are not regularly located, which makes it more challenging from a computational perspective. At the latent level, we follow Rigby and Stasinopoulos (2005) and use a generalized additive specification for the transformed location, scale and shape parameters of the data density. Our proposed model at the latent level contains catchment descriptors as covariates, e.g., catchment area and average annual rainfall, along with spatial model components for the transformed location and scale parameters, which are specified as approximate solutions to stochastic partial differential equations (SPDEs, see Lindgren et al. (2011)). These latent SPDE-based model components can capture complex spatially structured residuals more flexibly than the CAR priors of Sang and Gelfand (2009, 2010), while also yielding sparse precision matrices, which accelerates computations with large spatial datasets. Because the three parameters of the data level (i.e., the GEV location, scale and shape parameters) are transformed to the latent level, the proposed model is an LGM with a multivariate link function, referred to here as an extended LGM (Geirsson et al., 2015b). Our proposed link function keeps an intuitive interpretation and desirable properties for the shape parameter, while producing reliable estimates when several covariates are involved. Moreover, to prevent overfitting when multiple spatial random effects are involved, we specify relatively informative shrinkage priors for the most crucial hyperparameters, in order to penalize complex models that depart too much from a simpler counterpart (Simpson et al., 2017). Finally, instead of inferring our proposed extended LGM with an “exact” MCMC sampler as in Geirsson et al. (2015b), we here exploit an approximation to the posterior density adapted from the general methodology recently proposed by Hrafnkelsson et al. (2019), in order to better handle the high dimensionality of the data and to improve mixing and convergence of the MCMC chains. This fast Gaussian-based approximation of the posterior density makes it feasible to apply a 10-fold cross-validation experiment in order to select catchment descriptors for each of the three transformed parameters at the latent level. Furthermore, the computation of return levels (e.g., the 100-year event) is straightforward and their prediction at ungauged sites can be made efficiently through the posterior predictive distributions using site-specific covariates.

The paper is organized as follows. In Section 2, we present the data and covariates used in our statistical analysis. We then describe the specific flood frequency model in Section 3. In Section 4, we present the exact posterior density and its approximation, and we also introduce the method for selecting covariates for our flood frequency model. The results of the model selection and the posterior inference are presented and discussed in Section 5. The paper concludes with a discussion and perspectives for future research in Section 6.

2 Data and exploratory analysis

The data used in this paper come from the UK National River Flow Archive which is hosted by the Centre for Ecology & Hydrology on behalf of the Natural Environment Research Council; see National River Flow Archive (2018). The data consist of annual maxima from daily river flow observations measured at 554 gauging stations located across the UK. The observations date back to 1851 but most of the observations were made during the year from 1970 to 2013. A large fraction of the observational sites have between 50 and 80 annual maxima available. The dataset actually contains 958 gauging stations, but only stations that are deemed suitable for pooling and index flood calculations are used in our analysis. These stations are explicitly flagged as such in the original dataset. Figure 1 shows the location of the 554 stations along with the number of annual maxima available at each station.

The Anderson and Darling (1954) goodness-of-fit test, as presented by Stephens (1974), was

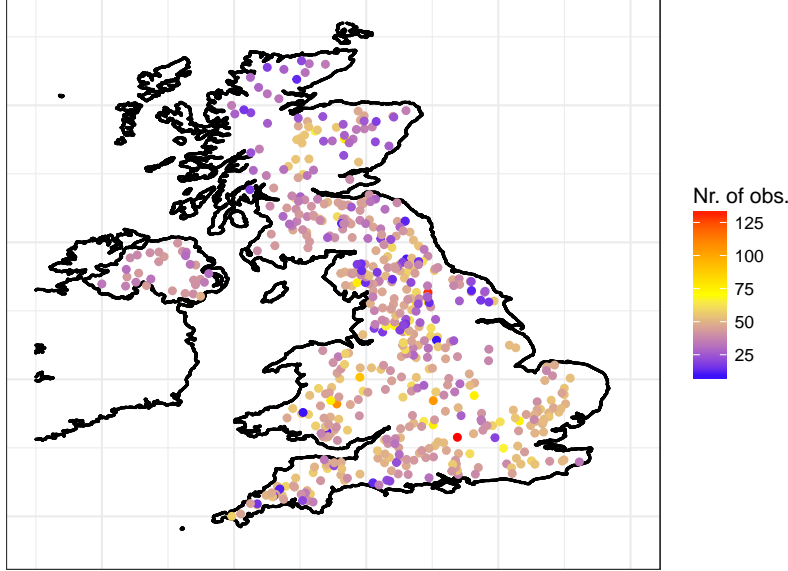


Figure 1: Map of the UK with the 554 stations used in our flood frequency analysis. The color bar indicates the number of annual maximum flow observations available at each station.

applied across the observational sites. It revealed that the GEV distribution is an appropriate model for the annual maxima data at all the sites; see the Supplementary Material for more details. This is no surprise, because the GEV distribution is the only possible limiting distribution for renormalized block maxima. The GEV distribution has by now a long tradition in the extreme-value literature and has been applied successfully in a wide range of applications; see, e.g., the book of Coles (2001), the review paper by Davison and Huser (2015), and references therein. The GEV cumulative distribution function may be expressed as

$$\text{GEV}(y \mid \mu, \sigma, \xi) = \begin{cases} \exp \left[- \{1 + \xi(y - \mu)/\sigma\}_+^{-1/\xi} \right], & \xi \neq 0; \\ \exp \left[- \exp \{-(y - \mu)/\sigma\} \right], & \xi = 0, \end{cases} \quad (1)$$

where $\mu \in \mathbb{R}$, $\sigma > 0$ and $\xi \in \mathbb{R}$ are location, scale and shape parameters, respectively, and $a_+ = \max(a, 0)$. The support of the GEV distribution is $[-\infty, \mu - \sigma/\xi]$, $[-\infty, +\infty]$, and $[\mu - \sigma/\xi, +\infty]$ when $\xi < 0$, $\xi = 0$, and $\xi > 0$, respectively, and the shape parameter ξ determines the tail heaviness, with a short, light and heavy upper tail when $\xi < 0$, $\xi = 0$, and $\xi > 0$, respectively.

In order to propose transformations for the GEV parameters μ , σ and ξ , we first explore their relationships as suggested by the data. To investigate this, we fitted the GEV distribution to all stations separately by maximum likelihood (ML). For completeness, we report these preliminary site-wise ML estimates in the Supplementary Material. The estimated location parameters are all positive and highly right-skewed, so we use the log transformation $\psi_i = \log(\mu_i)$ for all stations i in our Bayesian model specified below in Section 3. Moreover, the station-wise ML estimates suggest there is a clear positive linear relationship between the logarithms of the location and the scale parameters. Thus, we propose using the transformation $\tau_i = \log(\sigma_i/\mu_i)$. When modeling τ_i with covariates and a spatial effect, we can therefore capture the variability in the scale parameter that is not explained by the location parameter. The site-wise ML estimates of ξ suggest that

the underlying values of the shape parameter lie in the interval $(-0.5, 0.5)$. A suitable function that transforms values of ξ from the interval $(-0.5, 0.5)$ to the whole real line is motivated in Section 3.

The annual peak flow time series contain spatial information, and it appears that using this information is beneficial for accurate flood predictions. The spatial features in the location and scale of the data can be diagnosed by considering the variograms (Cressie, 1993) of the residuals of two basic linear models: the first model uses the median peak flow values from the sites as the dependent variables and the catchment descriptors as covariates, while the second model uses the interquartile range of the peak flow values as dependent variables; see the Supplementary Material for further details. The variograms indicate clearly that the residuals from the linear models for the location and scale statistics are spatially correlated. In conclusion, the location and scale parameters should be modeled as the sum of fixed covariate effects, a spatial model component, and an unstructured model component.

Catchment descriptors have previously been used to model extreme floods in the UK (e.g., Kjeldsen, 2010; Kjeldsen et al., 2017). In Table 1, we present all the catchment descriptors considered in this analysis. We selected a suitable transformation for each catchment descriptor on the basis of their empirical densities and their relationship with the ML estimates; see the caption of Table 1. Most of the catchment descriptors were log-transformed. For more details on the catchment descriptors, see Robson and Reed (1999).

The exploratory analysis briefly detailed above motivates the specification of our full Bayesian model, which is presented in the next section.

3 Model specification

We adopt a Bayesian framework to infer the parameters of the model for the annual maximum flow data. The Bayesian approach naturally handles simultaneous inference of multiple parameters, and allows us to incorporate latent random effects and prior information. Here we propose a novel Bayesian extended latent Gaussian model, where the latent level is composed of three generalized additive regression models for the transformed location, scale and shape parameters of the GEV density, and the models for the transformed location and scale parameters also contain spatial model components.

Let y_{it} be the annual maximum flow at station i in year t . The data from site i are assumed to be independent across years and to follow the GEV distribution with time-constant location parameter μ_i , scale parameter σ_i and shape parameter ξ_i , that is,

$$y_{it} \sim \text{GEV}(y_{it} | \mu_i, \sigma_i, \xi_i), \quad \mu_i, \sigma_i > 0, \quad \xi_i \in (-0.5, 0.5),$$

where for all y_{it} , $1 + \xi_i(y_{it} - \mu_i)/\sigma_i > 0$, $i \in \{1, \dots, J\}$, J is the number of sites, and $t \in \mathcal{A}_i$ where the set \mathcal{A}_i indexes the years for which observations are available at site i . Note that the domains of each parameter are restricted according to the findings of our exploratory analysis conducted in Section 2. Moreover, the data are assumed to be conditionally independent (spatially) given the latent GEV parameters. The following multivariate link function, g , is proposed for the parameters of the GEV density, namely,

$$(\psi_i, \tau_i, \phi_i) := g(\mu_i, \sigma_i, \xi_i) = (\log(\mu_i), \log(\sigma_i/\mu_i), h(\xi_i)) \in \mathbb{R}^3,$$

where

$$\phi_i = h(\xi_i) = a_\phi + b_\phi \log[-\log\{1 - (\xi_i + 1/2)^{c_\phi}\}],$$

with $a_\phi = 0.062376$, $b_\phi = 0.39563$ and $c_\phi = 0.8$. The function $h(\cdot)$ is motivated by four criteria: (i) The variance of the GEV distribution is assumed to be finite, leading to $\xi_i < 0.5$. (ii)

Table 1: Description of the catchment descriptors (covariates). The logarithmic function is used to transform these catchment descriptors except for BFIHOST, URBEXT and ASPBAR, which are transformed as BFIHOST^2 , $\log(\text{URBEXT} + 1)$ and $\text{ASPBAR}/100$, respectively.

Catchment descriptor	Description	Stats.		
		Min	Mean	Max
AREA	Catchment drainage area is the total area, in km^2 , where the river collects water [km^2].	1.63	440.65	9930.80
SAAR	Average annual rainfall [mm].	559.00	1114.12	2913.00
FARL	The Flood Attenuation by Reservoirs and Lakes index quantifies the degree of flood attenuation attributable to reservoirs and lakes in the catchment.	0.64	0.96	1.00
BFIHOST	A measure of catchment responsiveness.	0.17	0.49	0.97
FPEXT	Floodplain extent is the fraction of the total area of the catchment that is covered by the 100-year event.	0.00	0.06	0.30
URBEXT	Urban extent is an index that depicts the extent of urban/suburban land cover in the catchment area.	0.00	0.03	0.59
DPLBAR	Is the mean of the distances between each grid node and the catchment outlet [km].	1.30	23.05	139.87
DPSBAR	Mean drainage path slope provides an index of steepness in the catchment, [m/km].	13.30	100.12	441.80
LDP	Longest drainage path [km].	2.21	42.94	286.84
SPRHOST	Standard percentage runoff associated with each HOST soil class.	4.85	37.20	59.85
ASPBAR	The mean aspect or orientation of a catchment in degrees.	1.00	151.95	358.00
ALTBAR	The mean elevation of a catchment area [m].	25.00	220.78	682.00
ASPVAR	The aspect variance in the catchment in degrees.	0.02	0.17	0.59
PROPWET	An index for the proportion of time the soil in the catchment area is wet.	0.23	0.48	0.85

The upper bound of the GEV distribution when $\xi_i < 0$ is assumed to be larger than $\mu_i + 2\sigma_i$, leading to $\xi_i > -0.5$. This condition is also motivated by the regularity conditions of the ML estimator; see Smith (1985). (iii) The transformed parameter ϕ_i is such that its ML estimator has a variance that varies as little as possible for different values of ϕ_i corresponding to the interval $\xi_i \in (-0.3, 0.3)$. This is important when multiple covariates are used to model ϕ_i , in order to guarantee that each covariate will have the same effect on the model and to keep a separate interpretation. (iv) The transformation $h(\cdot)$ is finally chosen such that $h(0) = 0$ and the slope of $h(\xi)$ at $\xi = 0$ is equal to one (i.e., $h(\xi) \approx \xi$ for $\xi \approx 0$), so that ϕ keeps the same interpretation as ξ near zero. More details are given in the Supplementary Material.

Martins and Stedinger (2000) introduced a generalized maximum likelihood estimator as an alternative estimator in the frequentist setting for the parameters of the GEV distribution. The generalized maximum likelihood estimator is based on maximizing the generalized likelihood function defined as the product of the likelihood function and a prior density. For flood data, Martins and Stedinger (2000) argued that a beta density shifted to the interval $(-0.5, 0.5)$ with mean 0.10 and standard deviation 0.122 is a reasonable choice; see also Cooley and Sain (2010). Here we adopt a similar approach in our Bayesian inference by replacing the likelihood function with a generalized likelihood function that includes a prior density for each ϕ_i . These individual

prior densities at each site i are used in addition to the joint prior density defined at the latent level for all the ϕ parameters. We argued above that ξ should lie in $(-0.5, 0.5)$. In addition, exploring the ML estimates of ξ at each site (no prior density involved) showed that ξ is unlikely to lie outside the interval $(-0.3, 0.3)$. We therefore use a $\text{Beta}(\alpha, \beta)$ prior density shifted onto the interval $(-0.5, 0.5)$ for each ξ_i with parameters $\alpha = 4$ and $\beta = 4$, i.e., with mean zero and standard deviation 0.167. This beta prior density for each ξ_i is then transformed to a prior density for each ϕ_i . The estimates based on the mode of our proposed generalized likelihood function will simply be referred to as ML estimates hereafter.

At the latent level, our proposed generalized additive regression models for the three transformed parameters ψ , τ and ϕ may be expressed in vector notation as

$$\begin{aligned}\psi &= X_\psi \beta_\psi + A \mathbf{u}_\psi + \epsilon_\psi, \\ \tau &= X_\tau \beta_\tau + A \mathbf{u}_\tau + \epsilon_\tau, \\ \phi &= X_\phi \beta_\phi + \epsilon_\phi,\end{aligned}\tag{2}$$

where $\psi = (\psi_1, \dots, \psi_J)^\top$, $\tau = (\tau_1, \dots, \tau_J)^\top$ and $\phi = (\phi_1, \dots, \phi_J)^\top$. The design matrices X_ψ , X_τ and X_ϕ contain covariates, and β_ψ , β_τ and β_ϕ are the corresponding coefficients. The vectors \mathbf{u}_ψ and \mathbf{u}_τ are independent spatial random effects with Matérn correlation structure, modeled using finite-dimensional Gaussian Markov random fields (GMRF) via the stochastic partial differential equation (SPDE) approach of Lindgren et al. (2011). A review of certain types of SPDE models can be found in Bakka et al. (2018) and detailed case studies in Krainski et al. (2019). The SPDE approach requires a triangulated mesh defined over the region of interest, at which the continuous-space random field is approximated. The mesh constructed for our application is illustrated in Figure 2. The matrix A in (2) is a projection matrix that describes the projection

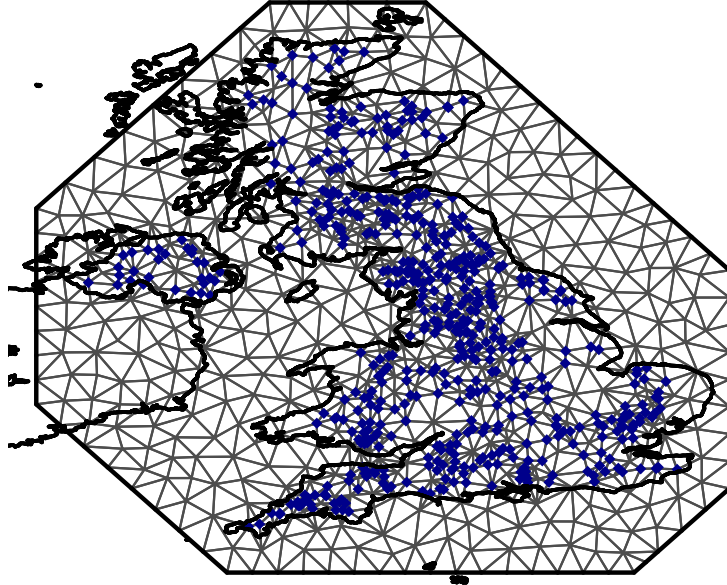


Figure 2: Triangulated mesh over the UK used to define the SPDE spatial model components at the latent level. The blue dots denote the observational sites.

from the representation of the GMRF on the mesh to the observational sites. The products, $A \mathbf{u}_\psi$

and $A\mathbf{u}_\tau$, are thus the effects of the spatial model components at the observational sites. The spatial model components \mathbf{u}_ψ and \mathbf{u}_τ are governed by two hyperparameters each, namely, the range parameters ρ_ψ and ρ_τ , and the marginal standard deviations, s_ψ and s_τ . The smoothness parameter (usually denoted by ν) of the Matérn correlation structure is here fixed to one, in order to produce reasonably smooth realizations.

The vectors $\boldsymbol{\epsilon}_\psi$, $\boldsymbol{\epsilon}_\tau$ and $\boldsymbol{\epsilon}_\phi$ in (2) contain unstructured zero-mean Gaussian model errors with variances $\sigma_{\epsilon_\psi}^2$, $\sigma_{\epsilon_\tau}^2$ and $\sigma_{\epsilon_\phi}^2$, respectively, sometimes called “nugget effects” in classical geostatistics. That is,

$$\boldsymbol{\epsilon}_\psi \sim \text{N}(0, \sigma_{\epsilon_\psi}^2 I), \quad \boldsymbol{\epsilon}_\tau \sim \text{N}(0, \sigma_{\epsilon_\tau}^2 I), \quad \boldsymbol{\epsilon}_\phi \sim \text{N}(0, \sigma_{\epsilon_\phi}^2 I),$$

where I is the identity matrix. All these error terms are assumed to be mutually independent, both spatially and across parameters.

The prior specifications of the unknown parameters are such that the covariate coefficients, $\boldsymbol{\beta}_\psi$, $\boldsymbol{\beta}_\tau$ and $\boldsymbol{\beta}_\phi$, and the spatial model components, \mathbf{u}_ψ and \mathbf{u}_τ , have Gaussian priors while the hyperparameters, σ_{ϵ_ψ} , σ_{ϵ_τ} , σ_{ϵ_ϕ} , s_ψ , s_τ , ρ_ψ and ρ_τ , are assigned penalized complexity (PC) priors to regularize the random effects of the model and shrink our complex Bayesian model towards a simpler reference model, thus preventing overfitting (Simpson et al., 2017). We use the same PC priors for $(s_\psi, \rho_\psi)^\top$ and $(s_\tau, \rho_\tau)^\top$ as in Fuglstad et al. (2018). Mutually independent prior densities are assumed for σ_{ϵ_ψ} , $(s_\psi, \rho_\psi)^\top$, σ_{ϵ_τ} , $(s_\tau, \rho_\tau)^\top$ and σ_{ϵ_ϕ} .

Combining the three equations in (2) together, the model at the latent level may be rewritten more compactly as

$$\boldsymbol{\eta} = Z\boldsymbol{\nu} + \boldsymbol{\epsilon}, \tag{3}$$

where

$$\begin{aligned} \boldsymbol{\eta} &= (\boldsymbol{\psi}^\top, \boldsymbol{\tau}^\top, \boldsymbol{\phi}^\top)^\top, \\ \boldsymbol{\nu} &= (\boldsymbol{\beta}_\psi^\top, \mathbf{u}_\psi^\top, \boldsymbol{\beta}_\tau^\top, \mathbf{u}_\tau^\top, \boldsymbol{\beta}_\phi^\top)^\top, \\ \boldsymbol{\epsilon} &= (\boldsymbol{\epsilon}_\psi^\top, \boldsymbol{\epsilon}_\tau^\top, \boldsymbol{\epsilon}_\phi^\top)^\top, \\ Z &= \begin{pmatrix} X_\psi & A_\psi & \cdot & \cdot & \cdot \\ \cdot & \cdot & X_\tau & A_\tau & \cdot \\ \cdot & \cdot & \cdot & \cdot & X_\phi \end{pmatrix}, \end{aligned}$$

where the dots denote zero entries.

In the next section, we describe how to fit this extended LGM to potentially large datasets, using an approximate Bayesian inference scheme.

4 Approximate posterior inference

4.1 Gaussian-based approximation to the posterior density

To deal with the high dimensionality of the data and the latent parameters, and to enable model selection at the latent level, a fast computational method for posterior inference is required. Hrafnkelsson et al. (2019) developed a general approximate posterior inference scheme for extended LGMs, which we exploit in our extreme-value framework. This approach is based on a Gaussian approximation to the likelihood function, which leads to a pseudo Gaussian–Gaussian model that is inferred instead of the initial extended LGM. This approximation is very accurate when numerous time replicates are available, and significantly facilitates inference, while also substantially reducing the computational burden (Hrafnkelsson et al., 2019).

To be more precise, let $\boldsymbol{\theta}$ be the vector containing the hyperparameters of the extended latent Gaussian model in Section 3, namely,

$$\boldsymbol{\theta} = (\theta_1, \dots, \theta_7)^\top = (\sigma_{\epsilon\psi}, s_\psi, \rho_\psi, \sigma_{\epsilon\tau}, s_\tau, \rho_\tau, \sigma_{\epsilon\phi})^\top.$$

Then, the posterior density can be written as

$$\begin{aligned} \pi(\boldsymbol{\eta}, \boldsymbol{\nu}, \boldsymbol{\theta} | \mathbf{y}) &\propto \pi(\boldsymbol{\theta}) \pi(\boldsymbol{\nu} | \boldsymbol{\theta}) \pi(\boldsymbol{\eta} | \boldsymbol{\nu}, \boldsymbol{\theta}) \pi(\mathbf{y} | \boldsymbol{\eta}) \\ &\propto \pi(\boldsymbol{\theta}) \pi(\boldsymbol{\nu} | \boldsymbol{\theta}) \pi(\boldsymbol{\eta} | \boldsymbol{\nu}, \boldsymbol{\theta}) L(\boldsymbol{\eta} | \mathbf{y}), \end{aligned} \quad (4)$$

where $L(\cdot | \cdot)$ denotes the generalized likelihood function. We then approximate the generalized likelihood function by a Gaussian density with mean $\hat{\boldsymbol{\eta}}$, and covariance matrix $\Sigma_{\eta y} = Q_{\eta y}^{-1}$, where $\hat{\boldsymbol{\eta}}$ is the mode of the (generalized) log-likelihood function and $Q_{\eta y}^{-1}$ is the inverse of the negative Hessian matrix of L evaluated at $\hat{\boldsymbol{\eta}}$. Let $\hat{L}(\boldsymbol{\eta} | \mathbf{y})$ be the Gaussian approximation to the generalized likelihood function. Denoting the approximation to the posterior density by $\hat{\pi}(\cdot | \cdot)$, we have

$$\begin{aligned} \hat{\pi}(\boldsymbol{\eta}, \boldsymbol{\nu}, \boldsymbol{\theta} | \mathbf{y}) &\propto \pi(\boldsymbol{\theta}) \pi(\boldsymbol{\nu} | \boldsymbol{\theta}) \pi(\boldsymbol{\eta} | \boldsymbol{\nu}, \boldsymbol{\theta}) \hat{L}(\boldsymbol{\eta} | \mathbf{y}) \\ &\propto \pi(\boldsymbol{\theta}) \pi(\boldsymbol{\nu} | \boldsymbol{\theta}) \pi(\boldsymbol{\eta} | \boldsymbol{\nu}, \boldsymbol{\theta}) \mathcal{N}(\boldsymbol{\eta} | \hat{\boldsymbol{\eta}}, Q_{\eta y}^{-1}). \end{aligned} \quad (5)$$

Now, consider a pseudo model that is such that $\hat{\boldsymbol{\eta}}$ (obtained by maximizing L at each site separately in a first step) is treated as the data, and assume that it follows the linear model in (3) used at the latent level of our original model. The proposed data density is now $\pi(\hat{\boldsymbol{\eta}} | \boldsymbol{\eta}) = \mathcal{N}(\hat{\boldsymbol{\eta}} | \boldsymbol{\eta}, Q_{\eta y}^{-1})$ where $Q_{\eta y}$ is as above and assumed to be known. The posterior density for this model can thus be written as

$$\begin{aligned} \pi(\boldsymbol{\eta}, \boldsymbol{\nu}, \boldsymbol{\theta} | \hat{\boldsymbol{\eta}}) &\propto \pi(\boldsymbol{\theta}) \pi(\boldsymbol{\eta}, \boldsymbol{\nu} | \boldsymbol{\theta}) \pi(\hat{\boldsymbol{\eta}} | \boldsymbol{\eta}) \\ &\propto \pi(\boldsymbol{\theta}) \pi(\boldsymbol{\eta}, \boldsymbol{\nu} | \boldsymbol{\theta}) \mathcal{N}(\hat{\boldsymbol{\eta}} | \boldsymbol{\eta}, Q_{\eta y}^{-1}) \\ &\propto \pi(\boldsymbol{\theta}) \pi(\boldsymbol{\eta}, \boldsymbol{\nu} | \boldsymbol{\theta}) \hat{L}(\boldsymbol{\eta} | \hat{\boldsymbol{\eta}}), \end{aligned} \quad (6)$$

where $\hat{L}(\boldsymbol{\eta} | \hat{\boldsymbol{\eta}}) = \hat{L}(\boldsymbol{\eta} | \mathbf{y})$. Hence, the above posterior density in (6) is the same as the Gaussian approximation (5) to the *exact* posterior density (4). The inference scheme used in this paper is based on inferring the pseudo model, which is a (fully conjugate) Gaussian–Gaussian model, and thus the posterior inference takes less computation time than the posterior inference for the exact model. Notice that once the estimates $\hat{\boldsymbol{\eta}}$ are obtained, the computational time required for fitting the pseudo model does no longer depend on the number of time replicates. Therefore, our proposed two-step inference approach benefits from large datasets with a lot of time replicates in two ways: not only the Gaussian approximation to the likelihood will become more accurate, but the computational return with respect to the “exact” Bayesian approach will also increase. We also emphasize here that although our inference approach is done in two consecutive steps (i.e., first estimating $\hat{\boldsymbol{\eta}}$, and second fitting the pseudo Gaussian–Gaussian model for $\hat{\boldsymbol{\eta}}$), the uncertainty in the first step is properly propagated into the second step.

The accuracy of the Gaussian approximation to i -th likelihood contribution $L(\boldsymbol{\eta}_i | \mathbf{y}_i)$, where $L(\boldsymbol{\eta} | \mathbf{y}) = \prod_{i=1}^J L(\boldsymbol{\eta}_i | \mathbf{y}_i)$, is illustrated in the Supplementary Material for various parameter settings. Our results show that the approximation becomes more accurate as the number of time replicates T increases. It is exceedingly accurate for the transformed location and shape parameters ψ_i and ϕ_i when $T = 50$ or $T = 80$ but has a slight negative bias for the transformed scale parameter τ_i in these temporal dimensions or for smaller T .

4.2 MCMC implementation and convergence diagnostics

All parameters of the pseudo model converged quickly using a Gibbs sampler with Metropolis steps with four chains each of length 10000 with a burn-in of 2000. The runtime on a standard laptop (2.6 GHz Intel Core i5, 8GB RAM, solid state hard drive), was approximately 26 hours when running the chains in parallel. The Gelman–Rubin statistic (Gelman and Rubin, 1992) is less than 1.1 for all the parameters, indicating adequate convergence to their respective stationary distributions, and trace plots and autocorrelation plots reveal that the chains mix well. There is no visible trend in the trace plots and the autocorrelation decreases rapidly for the latent parameters, and slightly less rapidly for the hyperparameters. The posterior densities of the model parameters are shown in the Supplementary Material along with trace plots of the MCMC chains, their autocorrelation plots, and convergence diagnostics based on the Gelman–Rubin statistic.

4.3 Model selection procedure based on INLA

For selecting parameters to use in the linear models for the transformed location, scale and shape parameters at the latent level, an additional approximation is performed, which is not used in the final inference procedure. For model selection purposes only, the pseudo Gaussian–Gaussian model is further simplified by setting the off-diagonal elements of $Q_{\eta y}^{-1}$ equal to zero, i.e., for a catchment i the covariances between $\hat{\psi}_i$ and $\hat{\tau}_i$, $\hat{\psi}_i$ and $\hat{\phi}_i$, and $\hat{\tau}_i$ and $\hat{\phi}_i$, at the data level, are set to zero, and only the marginal variances are considered. Specifically, the simplified version of the data density is thus

$$\pi(\hat{\boldsymbol{\eta}}|\boldsymbol{\eta}, \boldsymbol{\nu}, \boldsymbol{\theta}) = \mathcal{N}(\hat{\boldsymbol{\eta}}|\boldsymbol{\eta}, \text{diag}(Q_{\eta y}^{-1})).$$

The pseudo model for $\hat{\boldsymbol{\psi}}$ at the data level then takes the form

$$\pi(\hat{\boldsymbol{\psi}}|\boldsymbol{\psi}, \boldsymbol{\nu}, \boldsymbol{\theta}) = \mathcal{N}(\hat{\boldsymbol{\psi}}|\boldsymbol{\psi}, Q_{\psi y}^{-1}),$$

where $Q_{\psi y}^{-1}$ is the sample variance of $\hat{\boldsymbol{\psi}}$ obtained from $\text{diag}(Q_{\eta y}^{-1})$. Similarly, the pseudo models for $\hat{\boldsymbol{\tau}}$ and $\hat{\boldsymbol{\phi}}$ at the data level take the forms

$$\pi(\hat{\boldsymbol{\tau}}|\boldsymbol{\tau}, \boldsymbol{\nu}, \boldsymbol{\theta}) = \mathcal{N}(\hat{\boldsymbol{\tau}}|\boldsymbol{\tau}, Q_{\tau y}^{-1}) \quad \text{and} \quad \pi(\hat{\boldsymbol{\phi}}|\boldsymbol{\phi}, \boldsymbol{\nu}, \boldsymbol{\theta}) = \mathcal{N}(\hat{\boldsymbol{\phi}}|\boldsymbol{\phi}, Q_{\phi y}^{-1}).$$

This translates into assuming independence between the location, scale and shape parameters at the data level of the pseudo model such that the linear model for each of these three parameters can be tackled separately. This separation allows applying the integrated nested Laplace approximation (INLA) methodology (Rue et al., 2009) and exploiting the associated R package to estimate models independently for each of the three parameters, thus making a 10-fold cross-validation feasible. The INLA methodology bypasses MCMC sampling and the associated convergence assessment issues for LGMs with univariate link functions, by relying on a fast numerical approximation to the posterior density, which is similar in spirit (albeit with some important differences) to our proposed procedure detailed in Section 4.1 in the sense that it also exploits Gaussian-based approximations; for more details on INLA and its application to spatial models, see Bakka et al. (2018), and for an example of INLA applied to extreme precipitation data, see Opitz et al. (2018). The separate inference for $\boldsymbol{\psi}$, $\boldsymbol{\tau}$ and $\boldsymbol{\phi}$ is very efficient using INLA, taking 2, 2 and 1, minutes, respectively, on a standard laptop (same type as above). It is therefore possible to select the “best” covariates by cross-validation using a forward selection procedure

Table 2: The latent level of our final model. Model components (covariates or spatial effects) selected in our final model are indicated by check marks (\checkmark) for ψ , τ and ϕ .

Model component	ψ model	τ model	ϕ model
log(AREA)	\checkmark	\checkmark	
log(SAAR)	\checkmark	\checkmark	
log(FARL)	\checkmark	\checkmark	
log(FPEXT)		\checkmark	\checkmark
log(URBEXT + 1)		\checkmark	
BFIHOST ²	\checkmark		
Spatial component	\checkmark	\checkmark	

in a reasonable amount of time. The 10-fold cross-validation procedure that we used involves splitting the data into ten disjoint randomly chosen subsets with the same number of sites, the data from each site being used only once. The model is then trained on nine of those subsets and then used to predict the left-out subset and to compute the corresponding root mean squared prediction error. This step is repeated until each of the ten subsets have been used for testing, and the root mean squared prediction errors of each test set are then averaged to calculate the overall root mean squared prediction error (also simply called the “test error”) for a given model. In our application, the whole model selection procedure took only about 6 hours in total for all three parameters. As a result, linear models with good prediction properties were found for each of the three parameters. Moreover, in order to further motivate the inclusion of the spatial model components, the forward selection was performed with and without the spatial model components ψ and τ .

5 Results

5.1 Model selection results

We applied the forward model selection approach based on INLA described in Section 4.3 to select covariates for the linear models of ψ , τ and ϕ that are given by (2). Figure 3 shows the test error (i.e., the overall root mean squared prediction error) for the pseudo models fitted for ψ , τ and ϕ as a function of the number of covariates selected by the forward selection procedure as described in Section 4.3. In particular, the test error is significantly lower when spatial components for ψ and τ are included, which suggests that they should be included in the final model. Our results also show that the difference in test error is quite small after four, five and one covariate selected for ψ , τ and ϕ , respectively. The number of covariates chosen was determined by selecting the model with the smallest number of covariates that deviated less than 1% from the model with the smallest test error. Based on this rule we selected models for ψ , τ and ϕ with four, five and one covariate, respectively. All models also include an intercept. The model components (covariates and spatial effects) selected in our final models for ψ , τ and ϕ , respectively, are summarized in Table 2. The final models for ψ , τ use both the catchment area (AREA), the average annual rainfall (SAAR) and the flood attenuation index (FARL) as covariates. Additionally, the final model for ψ also uses the catchment responsiveness (BFIHOST), while the final model for τ also uses the floodplain extent (FPEXT) and the urban extent (URBEXT). The final model for ϕ uses the floodplain extent (FPEXT) as its only covariate. All covariates were transformed as

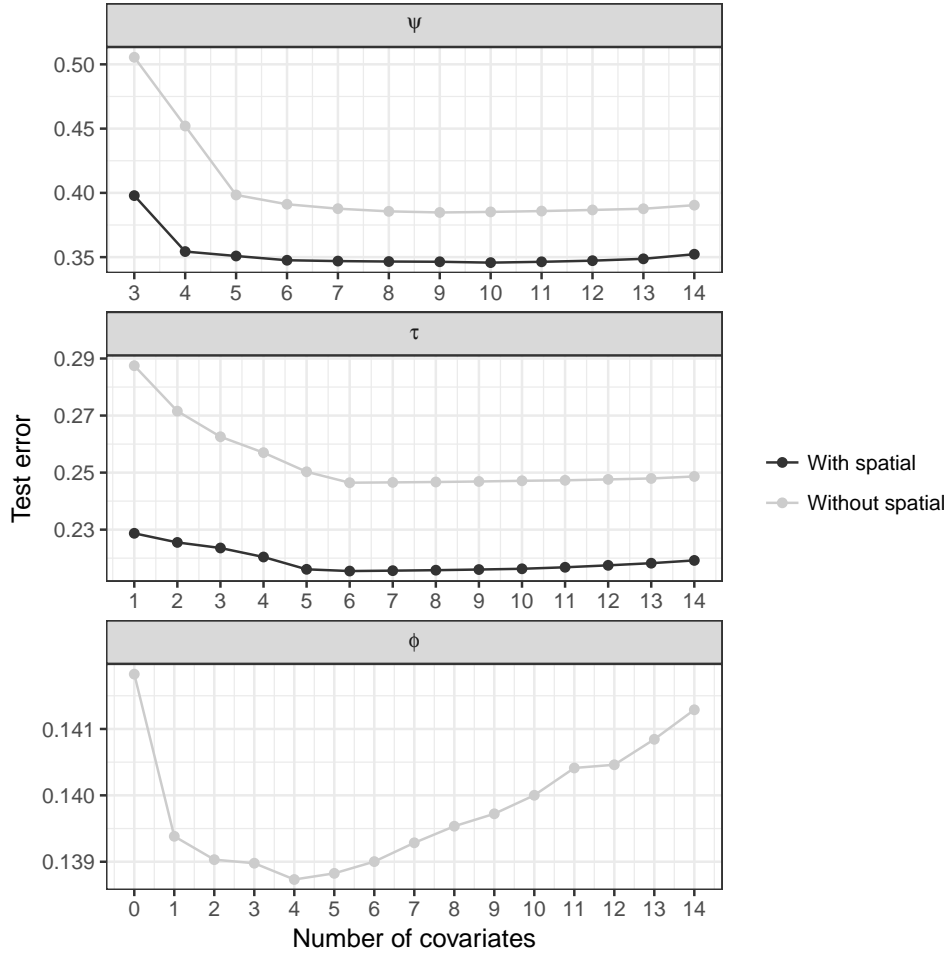


Figure 3: Test error (i.e., overall root mean squared prediction error) plotted as a function of the number of covariates selected by the forward selection procedure in the models for ψ , τ and ϕ (top to bottom). Black (respectively grey) curves correspond to models including (respectively not including) spatial structured model components at the latent level.

described in Table 1.

5.2 Parameter estimates and interpretation

Summary statistics for the hyperparameters are presented in the Supplementary Material. A comparison of the marginal standard deviations of the spatial model components and the unstructured model components of ψ and τ shows that the marginal standard deviations of the spatial model components are bigger than those of the random errors ϵ_ψ and ϵ_τ , which suggests that the inclusion of latent spatial random effects is helpful in borrowing strength across locations. Fitting simplified models to ψ and τ that do not contain spatial model components, similar to the models used for forward selection in the previous section using the same covariates as in the full model, resulted in the estimates $\sigma_{\psi\epsilon}^* = 0.397$ and $\sigma_{\tau\epsilon}^* = 0.211$. Here $\sigma_{\psi\epsilon}^*$ and $\sigma_{\tau\epsilon}^*$ denote the posterior means of the standard deviations of the unstructured model components in the simplified models for ψ and τ without the spatial component. This result is not surprising since

$$\sigma_{\psi\epsilon}^* = 0.397 \approx \sqrt{s_{\psi,\text{post}}^2 + \sigma_{\psi\epsilon,\text{post}}^2} = \sqrt{0.319^2 + 0.241^2} = 0.400$$

and

$$\sigma_{\tau\epsilon}^* = 0.211 \approx \sqrt{s_{\tau,\text{post}}^2 + \sigma_{\tau\epsilon,\text{post}}^2} = \sqrt{0.177^2 + 0.128^2} = 0.218,$$

where $s_{\psi,\text{post}}^2$, $\sigma_{\epsilon\psi,\text{post}}^2$, $s_{\tau,\text{post}}^2$ and $\sigma_{\epsilon\tau,\text{post}}^2$ denote the posterior means of s_ψ^2 , $\sigma_{\epsilon\psi}^2$, s_τ^2 and $\sigma_{\epsilon\tau}^2$, respectively, in the final model with the spatial model components. Thus, the calculations above show that the sum of the marginal variances of the spatial model components and the variances of the unstructured model components in the spatial model was approximately equal to the variances of the unstructured error terms in the model that did not have spatial model components. This suggests that the spatial model components explain variability that would otherwise not have been explained by the covariates. Figure 4 displays the posterior mean of the spatial model components of ψ and τ . The spatial model component of ψ takes values mainly between -0.5 and 0.5 which corresponds to a multiplication factor for μ that varies spatially between 0.61 at the lower end and 1.65 at the upper end. Similarly, the spatial model component of τ takes values mainly between -0.3 and 0.3 which translates into a multiplication factor for σ that varies spatially between 0.74 and 1.35 after taking μ into account. The spatial model component of τ has range parameter that is greater than the one of ψ by a factor two, and the effect of this can be seen in Figure 4. This indicates that there is a stronger spatial smoothing for the transformed scale parameter τ .

The original GEV location and scale parameters, μ and σ , can be written in terms of ψ and τ for station i as

$$\mu_i = \exp(\psi_i) = \exp(\mathbf{x}_{i,\psi}\boldsymbol{\beta}_\psi + \mathbf{a}_i\mathbf{u}_\psi + \epsilon_{\psi,i})$$

and

$$\sigma_i = \exp(\psi_i + \tau_i) = \exp(\mathbf{x}_{i,\psi}\boldsymbol{\beta}_\psi + \mathbf{x}_{i,\tau}\boldsymbol{\beta}_\tau + \mathbf{a}_i(\mathbf{u}_\tau + \mathbf{u}_\psi) + \epsilon_{\psi,i} + \epsilon_{\tau,i}).$$

Using the posterior means as point estimates for the covariates coefficients, the estimated location, scale and shape parameters may be expressed as

$$\begin{aligned} \mu_i = & e^{-12.019}(\text{AREA}_i)^{0.886}(\text{SAAR}_i)^{1.724}(\text{FARL}_i)^{3.705} \\ & \times e^{-3.228(\text{BFIHOST}_i)^2} e^{\mathbf{a}_i\mathbf{u}_\psi + \epsilon_{\psi,i}}, \end{aligned} \quad (7)$$

$$\begin{aligned} \sigma_i = & e^{-8.738}(\text{AREA}_i)^{0.831}(\text{SAAR}_i)^{1.077}(\text{FARL}_i)^{2.597} \\ & \times (\text{URBEXT}_i + 1)^{-0.661}(\text{FPEXT}_i)^{-0.129} e^{\mathbf{a}_i(\mathbf{u}_\psi + \mathbf{u}_\tau) + \epsilon_{\psi,i} + \epsilon_{\tau,i}}, \end{aligned} \quad (8)$$

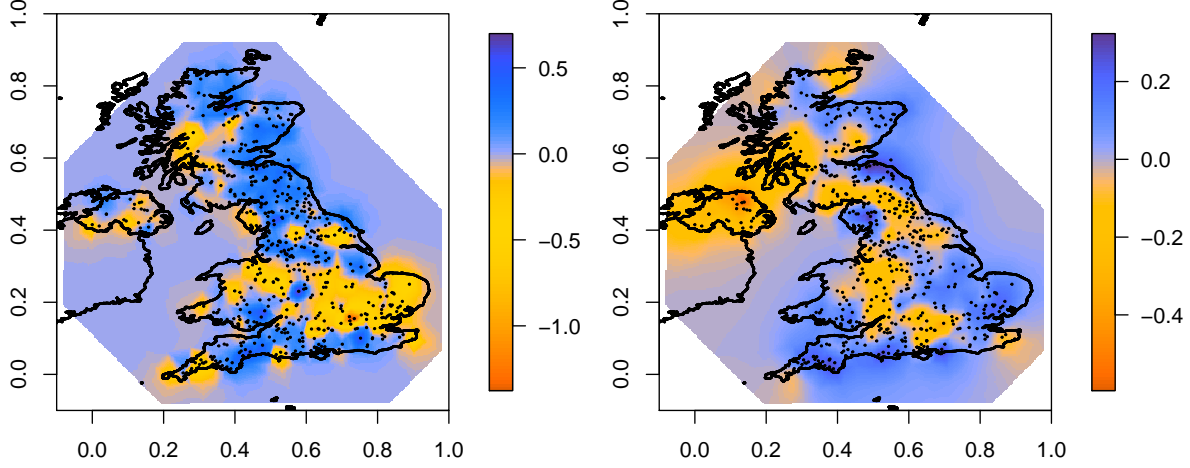


Figure 4: The posterior mean of the spatial model components of ψ (left) and τ (right).

$$\xi_i = \left[1 - \exp \left\{ - \exp \left(\frac{-0.102 - 0.037 \text{FPEXT}_i + \epsilon_{\phi,i} - a_\phi}{b_\phi} \right) \right\} \right]^{1/c_\phi} - \frac{1}{2}, \quad (9)$$

where $a_\phi = 0.062376$, $b_\phi = 0.39563$ and $c_\phi = 0.8$. The effect of a covariate that is used in both the ψ model and the τ model on σ needs to be handled in a particular way; for example, the effect of AREA on σ_i is governed by the exponent $\beta_{\psi,1} + \beta_{\tau,1}$ which is estimated to be 0.831 since the posterior estimates of $\beta_{\psi,1}$ and $\beta_{\tau,1}$ are 0.886 and -0.055 , respectively.

Figure 5 shows histograms of the posterior means of the GEV parameters, μ_i , σ_i and ξ_i , from all observational sites i along with the posterior means of the corresponding transformed parameters, ψ_i , τ_i and ϕ_i . The histograms of the preliminary site-wise ML estimates of the same parameters from these sites are shown in the Supplementary Material. Based on the posterior means of the shape parameters the data appear to be close to the Gumbel distribution with light tails as $\xi_i \approx 0$ at all sites i . Figure 6 shows the site-wise ML estimates of the GEV parameters and the transformed GEV parameters plotted against their final posterior means. The values of μ_i and σ_i vary a lot across catchments. Despite these large differences, our flexible spatial model can accurately capture the data distribution over space thanks to our choice of informative covariates and the inclusion of latent spatial model components and an unstructured model components. There is an excellent match between the preliminary site-wise ML estimates of the location parameter μ_i and their final model-based counterparts, and similarly (albeit to a less degree) for the scale parameter σ_i , and yet the uncertainty of the posterior estimates is substantially lower than the uncertainty associated with the ML estimates. This is due to spatial smoothing, and it implies that our Bayesian spatial model adequately borrows strength across locations for improving the estimation of μ_i and σ_i in the GEV distribution. There are, however, significant differences between the ML estimates and final model-based estimates of the shape parameter ξ_i . This is mainly due to shrinkage that is induced by the unstructured model component in the latent model for ϕ and the corresponding PC prior specified for its standard deviation, and as a result our Bayesian model improves the estimation of the shape parameter of the GEV distribution. Overall, there is therefore an excellent goodness-of-fit with a largely reduced estimation uncertainty compared to site-wise model fits.

A way to summarize the relative importance of covariates is to compare how the estimated GEV parameters μ , σ and ξ change as the corresponding covariates vary from the median

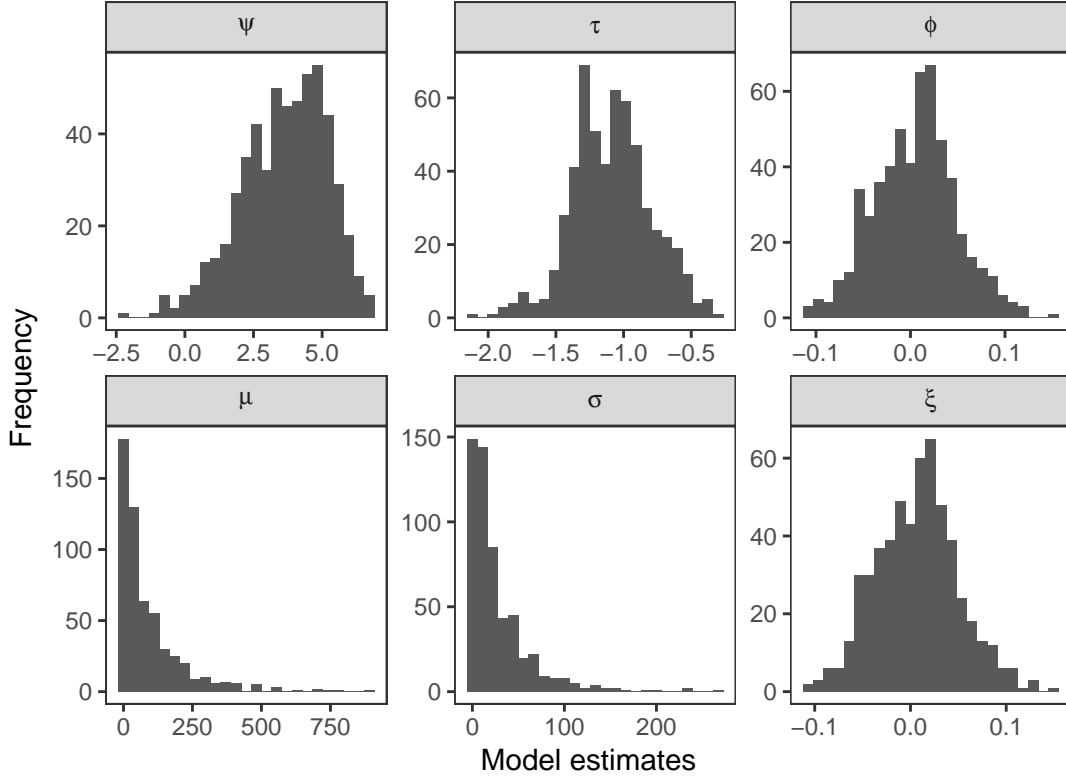


Figure 5: Histograms of the posterior means of the GEV parameters, μ , σ and ξ (bottom), from each of the observational sites along with the posterior means of the transformed GEV parameters, ψ , τ and ϕ (top).

to the first and third quartiles of their respective distributions. While the covariates have a multiplicative effect on μ and σ (see (7) and (8)), the only covariate involved in ξ (i.e., FPEXT) has an (approximate) additive effect on ξ thanks to the chosen link function $h(\xi)$ (see (9) and recall Section 3). Table 3 reports, for each covariate, the multiplicative and additive factors that affect the parameters μ_i , σ_i and ξ_i , when the value of a covariate varies from being equal to its median to being equal to its first and third quartiles, while keeping other covariates fixed and assuming that the spatial model component and the model error are equal. The parameters are set equal to their posterior means. For example, if μ_i and μ_j are such that the catchment area for station i is equal to the median (0.5-quantile) of AREA and station j has a catchment area equal to the third quartile (0.75-quantile) of AREA, but otherwise these two catchments have the same covariate values, spatial model component values and model error values, then $\mu_j = 2.081\mu_i$ (see the first row of Table 3). This indicates a substantial effect of the catchment drainage area. Notice that AREA has a major effect on both μ and σ . The second most important covariate is the average annual rainfall (SAAR), which makes a lot of sense. The other covariates have a more limited effect, despite still being significant (see the Supplementary Material for estimates and credible intervals for individual regression coefficients).

Table 3 also shows the effect of the spatial components on μ and σ . It can be shown that for two stations i and j , with the same covariate values and the same model error values, that are

Table 3: The effects of the covariates and the spatial model components in the final model on the location parameter, μ , the scale parameter, σ , the shape parameter, ξ , and the 100-year event (0.99 quantile) of the GEV density. The effect of a given covariate (or a given spatial model component) on μ is measured by comparing μ computed with the median value of the covariate (or the spatial model component) to μ computed with the 1st quartile and 3rd quartile of the covariate (or the spatial model component) while keeping other covariates and random effects fixed. The effect of the covariates (or the spatial model components) in the final model on σ , ξ and the 100-year event based on the same comparison is also given (in the case of ξ and the 100-year event, other covariates and random effects are set equal to their median values). For μ , σ and the 100-year event the effect is multiplicative, but for ξ the effect is (approximately) additive so the difference between predictions for the median and the quartiles is computed instead. Empty cells denote no effect while an asterisk (*) means that a comparison cannot be made.

Covariate	μ model		σ model		ξ model		100-year event	
	1st	3rd	1st	3rd	1st	3rd	1st	3rd
AREA	0.491	2.081	0.513	1.989			0.505	2.023
SAAR	0.663	1.574	0.774	1.327			0.732	1.419
FARL	0.889	1.058	0.920	1.040			0.908	1.047
BFIHOST	1.184	0.752					1.069	0.907
URBEXT			1.004	0.986			1.003	0.991
FPEXT			1.052	0.954	0.014	-0.013	1.054	0.954
Spatial ψ	0.843	1.175	0.843	1.175			0.843	1.175
Spatial τ			0.908	1.111			0.942	1.069
Spatial $\psi + \tau$	*	*	0.824	1.243			*	*

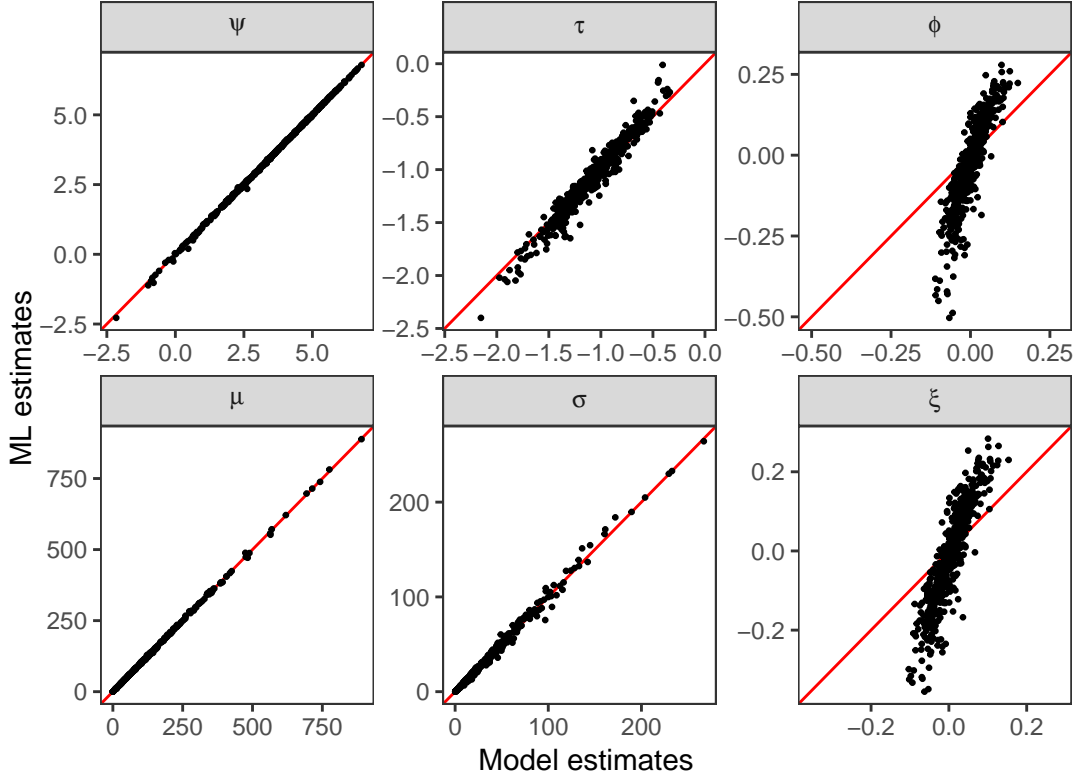


Figure 6: The ML estimates of the GEV parameters, μ , σ and ξ (bottom), and their transformations, ψ , τ and ϕ (top), as a function of their posterior estimates.

located at different places, the ratio of the expected location parameter at station i and station j , can be written as

$$\frac{\mu_j}{\mu_i} = \frac{\exp(\mathbf{a}_j \mathbf{u}_\psi)}{\exp(\mathbf{a}_i \mathbf{u}_\psi)}.$$

Table 3 shows this ratio when $\mathbf{a}_i \mathbf{u}_\psi$ is the median of the spatial model component for ψ and $\mathbf{a}_j \mathbf{u}_\psi$ is either the lower or upper quartile of the spatial model component for ψ . The sizes of the ratios are 0.843 (the lower quartile over the median) and 1.175 (the upper quartile over the median), and, e.g., the latter can be interpreted as the multiplicative effect of the spatial model component for ψ relative to its upper quartile and its median. Note that the above ratio is not effected by the spatial model component for τ .

The ratio of the expected scale parameters at stations i and j , can be written in as

$$\frac{\sigma_j}{\sigma_i} = \frac{\exp(\mathbf{a}_j \mathbf{u}_\psi + \mathbf{a}_j \mathbf{u}_\tau)}{\exp(\mathbf{a}_i \mathbf{u}_\psi + \mathbf{a}_i \mathbf{u}_\tau)}.$$

Table 3 shows this ratio when $\mathbf{a}_i \mathbf{u}_\tau$ is the median of the spatial model component for τ and $\mathbf{a}_j \mathbf{u}_\tau$ is either the lower or upper quartile of the spatial model component for τ . This ratio is also evaluated with respect to the spatial model component for ψ , and it has the same effect on σ and μ . The multiplicative effect of the spatial model component for τ on σ relative to its

upper quartile and its median is 1.111. The joint effect of the spatial model components \mathbf{u}_ψ and \mathbf{u}_τ on the above ratio is also given in Table 3 but its effect on the ratio for μ is not meaningful and thus not reported.

To investigate the effect of model components on extreme events, e.g., the 100-year event, the corresponding quantiles need to be estimated. The quantile function of the GEV distribution has an explicit expression, which makes it straightforward to compute. Inverting (1), the expression for the p -quantile is

$$Q(p|\mu, \sigma, \xi) = \begin{cases} \mu + \sigma\{-\log(p)\}^{-\xi} - 1/\xi & \xi \neq 0, \\ \mu - \sigma \log\{-\log(p)\} & \xi = 0, \end{cases} \quad p \in (0, 1),$$

and the 100-year event corresponds to $Q(0.99|\mu, \sigma, \xi)$. The multiplication effects of the covariates and the spatial model components on the 100-year event are given in Table 3. Again, the parameters are set equal to their posterior means. The unstructured model components, ϵ_ψ , ϵ_τ and ϵ_ϕ , and the spatial model components, \mathbf{u}_ψ and \mathbf{u}_τ , are set equal to zero when the effects of the covariates are quantified. Table 3 shows how the 100-year event changes when covariates or spatial model components vary from their median values to their lower or upper quartiles. As above, AREA appears to be the most important covariate, followed by SAAR.

We then illustrate the estimates of return levels and annual maximum flow distributions at three randomly selected stations. The top panel of Figure 7 shows the posterior means of return levels as a function of the return period, with associated 95% credible intervals, and we also display the order statistics for each station with their associated uncertainty (i.e., 95% prediction intervals). Notice that the x-axis is expressed on a log-scale. The bottom panel of Figure 7 shows the empirical distribution of the observed annual maxima of the three stations and the posterior mean of the distribution along with 95% credible bands. The relatively good match between the posterior distributions and the empirical distributions indicates that our model fits well overall. Similar results (not shown) were obtained for the other stations. Moreover, by comparing the uncertainty bands in the top panel of Figure 7, we can see that the uncertainty of our model-based estimates is quite moderate compared to the uncertainty of the (empirical) order statistics.

Finally, Figure 8 shows the posterior predictive density at six observational stations which were randomly selected from stations having more than 40 available observations. The six stations were removed from the dataset and the remaining data were used to infer the parameters and estimate the posterior predictive density using the covariates at the six stations. Figure 8 shows that the predictive density captures the real observations quite well. As expected, the standard deviation of the posterior predictive densities is slightly larger than the sample standard deviation of the observations.

6 Discussion

In this paper, we developed an extended latent Gaussian model based on the generalized extreme-value distribution, designed for flood frequency analyses, and we illustrated our approach by application to a large dataset of maximum annual peak flow time series from the UK. Because of the large dimensionality of the data and the high model complexity, GMRF priors were assumed for latent spatial effects, and an approximation was made to the posterior density following the recent contribution of Hrafnkelsson et al. (2019) to simplify and speed up posterior inference for latent Gaussian models. This approximation boils down to fitting a pseudo Gaussian-Gaussian model that is used to make inference on the model parameters. The covariates for the final

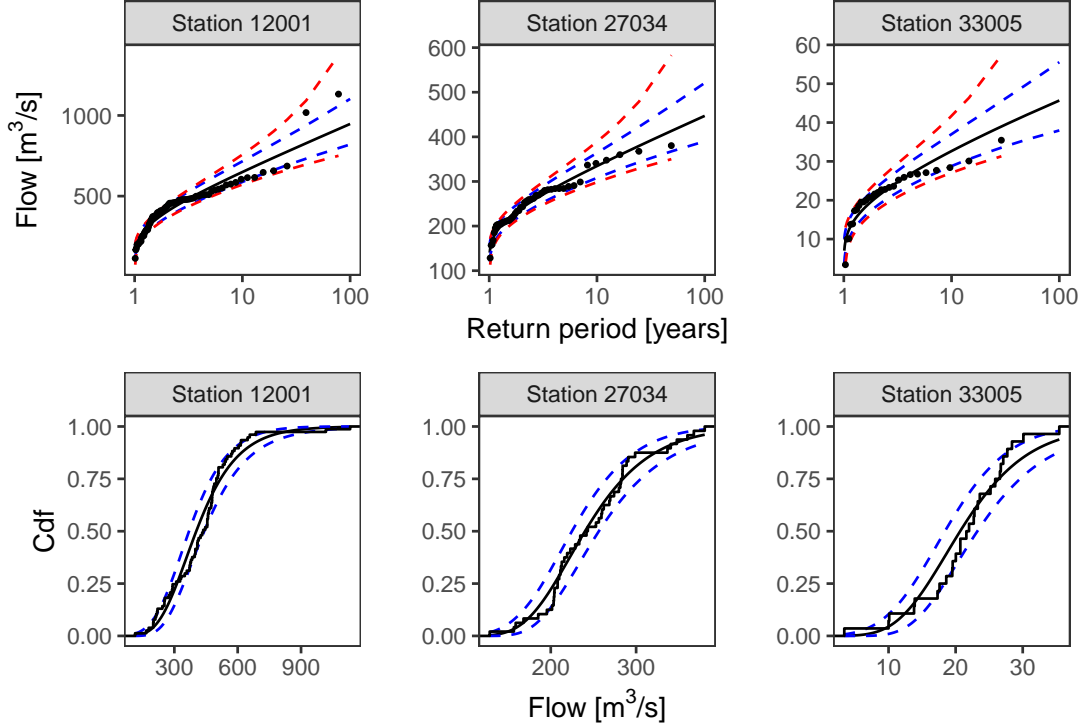


Figure 7: Top row: Estimates (i.e., posterior means (solid black line)) of return levels as a function of the return period for three randomly selected stations. The blue dashed lines show 95% credible intervals for the return levels. The ordered observations as a function of return period (black points) are shown along with 95% prediction intervals for the ordered observations (red dashed lines), which represent the variability of the order statistics. Bottom row: Empirical (black step-like curves) and fitted (solid black lines) cumulative distribution functions of the annual maximum flow data along with 95% credible intervals (blue dashed lines) for the fitted cumulative distribution functions.

model were selected with a simplified model setup that allowed us to use INLA which led to a substantial reduction in the computation time. The selected covariates were significant in the final model, i.e., their 95% posterior intervals did not include zero.

How to parameterize the GEV distribution within a Bayesian hierarchical model is an important and challenging methodological question. In this paper a novel multivariate link function for the three parameters of the GEV distribution was proposed. A standard logarithmic transformation was used for the location μ , and the confounding between the location μ and scale σ was dealt with by transforming them jointly. We proposed a novel transformation for ξ that was constructed based on four criteria that we believe are reasonable when inferring of the tail behaviour of flood data with the GEV distribution. Moreover, the new transformation stabilized the inference of ξ .

The proposed model was inferred with a Bayesian approach and the data were not transformed before inferring the parameters and thus their uncertainty was properly quantified. Normalisation is required for some commonly used flood frequency models such as the index flood method and

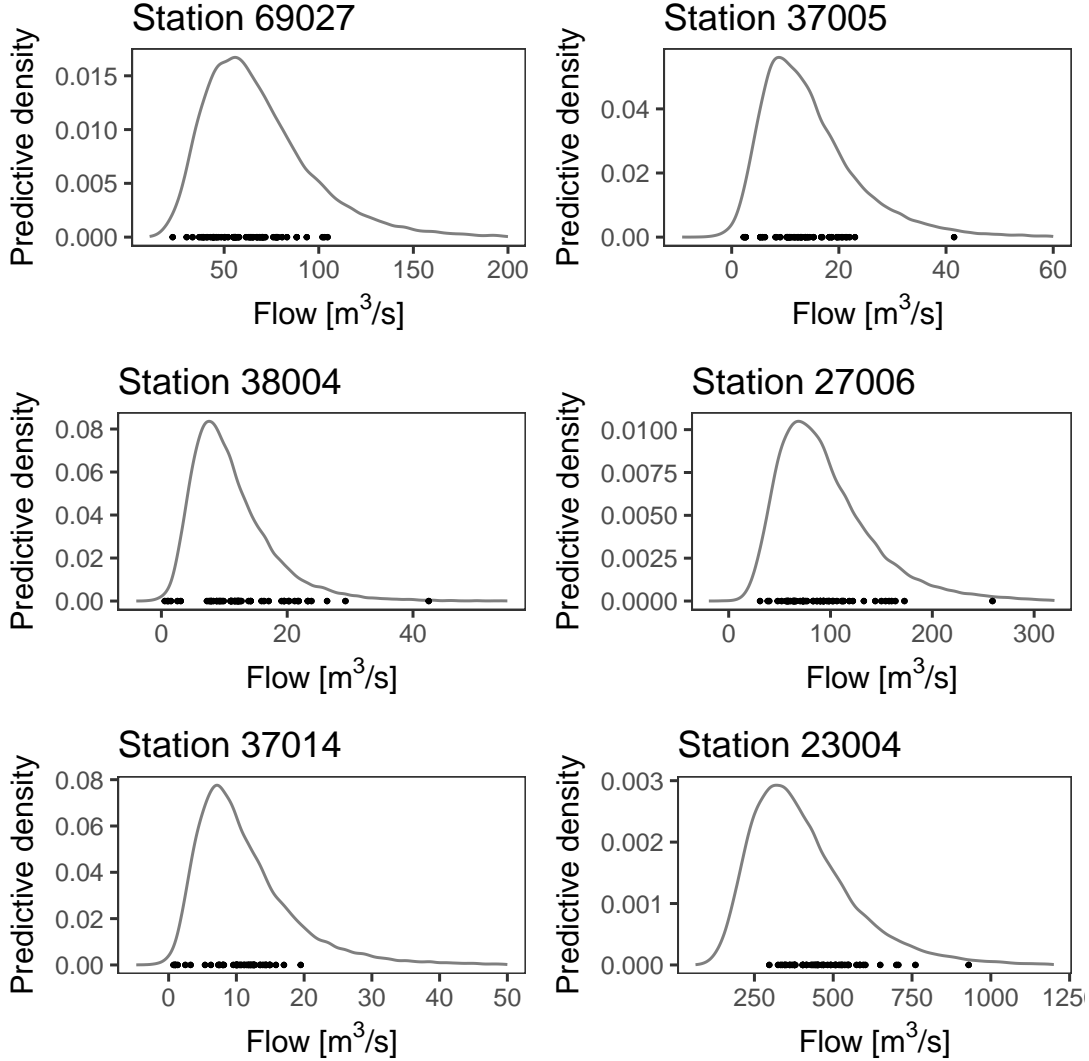


Figure 8: The posterior predictive density at six observational stations and the real observations of those stations. These six stations were randomly selected from stations having more than 40 available observations and then removed from the dataset before their posterior predictive densities were evaluated.

as a consequence uncertainty is not properly propagated. Under the extended LGM framework used here, it was straightforward to include covariates and additional random effects at the latent level and keep track of the uncertainty of the model parameters. PC prior densities were defined for the hyperparameters of the model. The hyperparameters in the extended LGM setup govern the latent parameters which are a part of an additive regression model, and thus the penalization of increased complexity becomes essential to regularize the random effects at the latent level.

The results showed that all parameters of the model converged quickly and most parameters were well defined, in particular, the hyperparameters, which all had small posterior standard

deviations with respect to their posterior means. The results showed that the spatial model components for ψ and τ explained more than half of the otherwise unexplained variability, which indicates that they are essential in our model. The return period of extreme floods was investigated by computing quantiles of the fitted GEV distribution and taking their uncertainty into account. Posterior predictive distributions were computed for six gauging stations and our results showed that our proposed model is useful for predicting extreme flow data within ungauged catchments.

Our analysis demonstrates that the LGM framework is very flexible and powerful for predicting extreme flow data within gauged and ungauged catchments, by efficiently borrowing strength across locations. However, the underlying conditional independence assumption of the data with respect to latent parameters makes it unsuitable when dependence across catchments is present and predictions on the joint behavior of the catchments are needed. Sang and Gelfand (2010) suggested relaxing the conditional independence assumption by using a Gaussian dependence structure at the data level, but this approach does not properly capture extremal dependence. For this purpose, more complex and specialized extreme-value models are required. In the case of strong extremal dependence, max-stable processes (Padoan et al., 2010; Davison et al., 2012; Huser and Davison, 2014; Asadi et al., 2015; Vettori et al., 2019; Davison et al., 2019) have proven to be useful for modeling spatial block maxima, while in the case of weakening extremal dependence, broader classes of max-infinitely divisible processes (Huser et al., 2018; Bopp et al., 2019) have recently been proposed. These models, however, are usually much more intensive to fit than our proposed extended LGM and further research is needed to make them attractive in large dimensions as in this paper.

We believe that our proposed latent Gaussian model and its inference scheme have features that are important for flood frequency analysis in general. In particular, predictions of extreme events in the case of both gauged and ungauged catchments are improved due to (i) reducing the uncertainty in the shape parameter by transforming it and regularizing the transformed parameter with an unstructured model component; (ii) modeling the location and scale parameters spatially and utilizing the correlation between these two parameters; (iii) applying the fast approximated inference scheme, making it possible to evaluate large number of potential regression models and to perform extensive cross-validation to achieve good prediction properties. In our view future research efforts in flood frequency analysis should focus on the development of fast inference schemes for models that take extremal dependence into account.

References

- T.W. Anderson, D.A. Darling, A test of goodness of fit. *Journal of the American Statistical Association* **49**(268), 765–769 (1954)
- P. Asadi, A.C. Davison, S. Engelke, Extremes on river networks. *The Annals of Applied Statistics* **9**(4), 2023–2050 (2015). doi:10.1214/15-aos863
- H. Bakka, H. Rue, G.-A. Fuglstad, A. Riebler, D. Bolin, J. Illian, E. Krainski, D. Simpson, F. Lindgren, Spatial modeling with R-INLA: A review. *Wiley Interdisciplinary Reviews: Computational Statistics* **10**(6), 1443 (2018). doi:10.1002/wics.1443
- G. Bopp, B.A. Shaby, R. Huser, 2019, A hierarchical max-infinitely divisible process for extreme areal precipitation over watersheds. arXiv preprint 1805.06084
- D.H. Burn, Evaluation of regional flood frequency analysis with a region of influence approach. *Water Resources Research* **26**(10), 2257–2265 (1990). doi:10.1029/WR026i010p02257

- S.G. Coles, *An Introduction to Statistical Modeling of Extreme Values* (Springer, London, 2001). ISBN 9781852334598
- D. Cooley, S.R. Sain, Spatial hierarchical modeling of precipitation extremes from a regional climate model. *Journal of Agricultural, Biological, and Environmental Statistics* **15**(3), 381–402 (2010)
- N.A. Cressie, *Statistics for Spatial Data* (Wiley, New York, 1993)
- C. Cunnane, J. Nash, Bayesian estimation of frequency of hydrological events. *Mathematical Models in Hydrology* **1** (1974)
- T. Dalrymple, Flood-frequency analyses, *Manual of Hydrology: Part 3*, Technical report, US-GPO, 1960
- A.C. Davison, R. Huser, E. Thibaud, Spatial extremes, in *Handbook of Environmental and Ecological Statistics*, ed. by A.E. Gelfand, M. Fuentes, J.A. Hoeting, R.L. Smith (CRC press, Boca Raton, 2019)
- A.C. Davison, R. Huser, Statistics of Extremes. *Annual Review of Statistics and its Application* **2**, 203–235 (2015). doi:10.1146/annurev-statistics-010814-020133
- A.C. Davison, S. Padoan, M. Ribatet, Statistical Modelling of Spatial Extremes (with Discussion). *Statistical Science* **27**(2), 161–186 (2012). doi:10.1214/11-STS376
- A.V. Dyrddal, A. Lenkoski, T.L. Thorarinsdottir, F. Stordal, Bayesian hierarchical modeling of extreme hourly precipitation in Norway. *Environmetrics* **26**, 89–106 (2015). doi:10.1002/env.2301
- G.-A. Fuglstad, D. Simpson, F. Lindgren, H. Rue, Constructing priors that penalize the complexity of Gaussian random fields. *Journal of the American Statistical Association* **114**(525), 445–452 (2018). doi:10.1080/01621459.2017.1415907
- Ó.P. Geirsson, B. Hrafnkelsson, D. Simpson, Computationally efficient spatial modeling of annual maximum 24-h precipitation on a fine grid. *Environmetrics* **26**(5), 339–353 (2015a). doi:10.1002/env.2343
- Ó.P. Geirsson, B. Hrafnkelsson, D. Simpson, H. Sigurðarson, The MCMC split sampler: A block Gibbs sampling scheme for latent Gaussian models. arXiv preprint 1506.06285 (2015b)
- A. Gelman, D.B. Rubin, Inference from iterative simulation using multiple sequences. *Statistical Science*, 457–472 (1992). doi:10.1214/ss/1177011136
- GREHYS, Presentation and review of some methods for regional flood frequency analysis. *Journal of Hydrology (Amsterdam)* **186**(1-4), 63–84 (1996). doi:10.1016/S0022-1694(96)03042-9
- J.R.M. Hosking, J.R. Wallis, *Regional frequency analysis: an approach based on L-moments* (Cambridge University Press, Cambridge, 2005). ISBN 9780521430456
- J.R. Hosking, J.R. Wallis, E.F. Wood, Estimation of the generalized extreme-value distribution by the method of probability-weighted moments. *Technometrics* **27**(3), 251–261 (1985)

- B. Hrafnkelsson, J.S. Morris, V. Baladandayuthapani, Spatial modeling of annual minimum and maximum temperatures in Iceland. *Meteorology and Atmospheric Physics* **116**(1-2), 43–61 (2012). doi:10.1007/s00703-010-0101-0
- B. Hrafnkelsson, A.J. Johannesson, S. Siegert, H. Bakka, R. Huser, Approximate posterior inference for latent Gaussian models with multivariate link functions. arXiv preprint 1906.xxxxx (2019)
- G. Huerta, B. Sansó, Time-varying models for extreme values. *Environmental and Ecological Statistics* **14**(3), 285–299 (2007). doi:10.1007/s10651-007-0014-3. <https://doi.org/10.1007/s10651-007-0014-3>
- R. Huser, A.C. Davison, Space-time modelling of extreme events. *Journal of the Royal Statistical Society (Series B)* **76**(439–461) (2014). doi:10.1111/rssb.12035
- R. Huser, T. Opitz, E. Thibaud, 2018, Max-infinitely divisible models and inference for spatial extremes. arXiv preprint 1801.02946
- J. Jalbert, A.-C. Favre, C. Bélisle, J.-F. Angers, A spatiotemporal model for extreme precipitation simulated by a climate model, with an application to assessing changes in return levels over North America. *Journal of the Royal Statistical Society (Series C)* **66**(5), 941–962 (2017)
- T.R. Kjeldsen, Modelling the impact of urbanization on flood frequency relationships in the UK. *Hydrology Research* **41**(5), 391–405 (2010). doi:10.2166/nh.2010.056
- T.R. Kjeldsen, D.A. Jones, Prediction uncertainty in a median-based index flood method using L moments. *Water Resources Research* **42**(7) (2006). doi:10.1029/2005WR004069
- T.R. Kjeldsen, D.A. Jones, An exploratory analysis of error components in hydrological regression modeling. *Water Resources Research* **45**(2) (2009a). doi:10.1029/2007WR006283
- T.R. Kjeldsen, D.A. Jones, A formal statistical model for pooled analysis of extreme floods. *Hydrology Research* **40**(5), 465–480 (2009b). doi:10.2166/nh.2009.055
- T.R. Kjeldsen, H. Ahn, I. Prosdocimi, On the use of a four-parameter kappa distribution in regional frequency analysis. *Hydrological Sciences Journal* **62**(9), 1354–1363 (2017). doi:10.1080/02626667.2017.1335400
- E.T. Krainski, V. Gómez-Rubio, H. Bakka, A. Lenzi, D. Castro-Camilio, D. Simpson, F. Lindgren, H. Rue, *Advanced Spatial Modeling with Stochastic Partial Differential Equations using R and INLA* (Chapman and Hall/CRC, New York, 2019). Github version www.r-inla.org/spde-book. doi:10.1201/9780429031892
- G. Kuczera, Comprehensive at-site flood frequency analysis using Monte Carlo Bayesian inference. *Water Resources Research* **35**(5), 1551–1557 (1999). doi:10.1029/1999WR900012
- F. Lindgren, H. Rue, J. Lindström, An explicit link between Gaussian fields and Gaussian Markov random fields: the stochastic partial differential equation approach. *Journal of the Royal Statistical Society: Series B (Statistical Methodology)* **73**(4), 423–498 (2011). doi:10.1111/j.1467-9868.2011.00777.x
- E.S. Martins, J.R. Stedinger, Generalized maximum-likelihood generalized extreme-value quantile estimators for hydrologic data. *Water Resources Research* **36**(3), 737–744 (2000). doi:10.1029/1999WR900330

- National River Flow Archive, 2018. NERC CEH, Wallingford. <https://nrfa.ceh.ac.uk>
- T. Opitz, R. Huser, H. Bakka, H. Rue, INLA goes extreme: Bayesian tail regression for the estimation of high spatio-temporal quantiles. *Extremes* **21**(3), 441–462 (2018). doi:10.1007/s10687-018-0324-x
- S.A. Padoan, M. Ribatet, S.A. Sisson, Likelihood-based inference for max-stable processes. *Journal of the American Statistical Association* **105**(489), 263–277 (2010). doi:10.1198/jasa.2009.tm08577
- R.A. Rigby, D.M. Stasinopoulos, Generalized additive models for location, scale and shape. *Journal of the Royal Statistical Society: Series C (Applied Statistics)* **54**(3), 507–554 (2005). doi:10.1111/j.1467-9876.2005.00510.x
- A. Robson, D. Reed, Flood estimation handbook. Institute of Hydrology, Wallingford (1999)
- D. Rosbjerg, H. Madsen, Uncertainty measures of regional flood frequency estimators. *Journal of Hydrology* **167**(1-4), 209–224 (1995). doi:10.1016/0022-1694(94)02624-K
- H. Rue, S. Martino, N. Chopin, Approximate Bayesian inference for latent Gaussian models by using integrated nested Laplace approximations. *Journal of the Royal Statistical Society: Series B (Statistical Methodology)* **71**(2), 319–392 (2009). doi:10.1111/j.1467-9868.2008.00700.x
- H. Sang, A.E. Gelfand, Hierarchical modeling for extreme values observed over space and time. *Environmental and Ecological Statistics* **16**(3), 407–426 (2009). doi:10.1007/s10651-007-0078-0. <https://doi.org/10.1007/s10651-007-0078-0>
- H. Sang, A.E. Gelfand, Continuous spatial process models for spatial extreme values. *Journal of Agricultural, Biological, and Environmental Statistics* **15**(1), 49–65 (2010). doi:10.1007/s13253-009-0010-1. <https://doi.org/10.1007/s13253-009-0010-1>
- D. Simpson, H. Rue, A. Riebler, T.G. Martins, S.H. Sørbye, et al., Penalising model component complexity: A principled, practical approach to constructing priors. *Statistical Science* **32**(1), 1–28 (2017). doi:10.1214/16-STS576
- R.L. Smith, Maximum likelihood estimation in a class of nonregular cases. *Biometrika* **72**(1), 67–90 (1985). doi:10.2307/2336336
- M.A. Stephens, Edf statistics for goodness of fit and some comparisons. *Journal of the American statistical Association* **69**(347), 730–737 (1974)
- T.L. Thorarinsdottir, K.H. Hellton, G.H. Steinbakk, L. Schlichting, K. Engeland, Bayesian regional food frequency analysis for large catchments. arXiv preprint 1802.09278 (2018)
- S. Vettori, R. Huser, M.G. Genton, Bayesian modeling of air pollution extremes using nested multivariate max-stable processes. *Biometrics* (2019). To appear.

Supplementary Material for the paper “Approximate Bayesian inference for spatial flood frequency analysis”

Árni V. Johannesson,¹ Birgir Hrafnkelsson,^{1*} Raphaël Huser,²
Haakon Bakka², Stefan Siegert³

¹University of Iceland,

²King Abdullah University of Science and Technology

³University of Exeter

1 Details of the statistical model

1.1 General comments

In Geirsson et al. (2015) and Thorarinsdottir et al. (2018), the GEV distribution is applied to data on annual maximum 24-h precipitation from Iceland and annual maximum floods from Norway, respectively. The parameters of the GEV distribution are transformed in the same way in these two papers, namely, the scale parameter is transformed with the logarithmic function; the location and shape parameters are transformed with the identity link; and in both papers covariates are used while spatial models for the parameters are only used in Geirsson et al. (2015). The model presented below corresponds to the model applied in the main paper. It is a modified version of the models in Geirsson et al. (2015) and Thorarinsdottir et al. (2018). In the model presented in the main paper, the location parameter is transformed with the logarithmic function and the scale parameter is transformed by taking the logarithm of the ratio of the scale parameter and the location parameter. Both of these transformations are modeled at the latent level and both of them include a spatial model component. Furthermore, the shape parameter of the GEV distribution, ξ , is assumed to lie in the interval $(-0.5, 0.5)$. It is transformed from the interval $(-0.5, 0.5)$ to the real line with a novel transformation, see Section 1.2.

1.2 A transformation for the shape parameter

The transformed shape parameter is denoted by $\phi = h(\xi)$. The selection of the transforming function h for the shape parameter ξ is based on several criteria. The first criterion is that the variance of the data distribution describing the floods, that is, the GEV distribution, is finite, leading to the constraint $\xi < 0.5$. The second criterion is a moderate upper bound of the GEV distribution when $\xi < 0$. Here we opt for $\xi > -0.5$ which leads to upper bounds equal to $\mu + c_\xi \sigma$ where $c_\xi \geq 2$. This is partially motivated by looking at estimates of the shape parameter at each site in the UK flood dataset. Notice that this constraint also implies that the score function has finite variance and that the maximum likelihood (ML) estimator has the usual asymptotic behavior (Smith, 1985). The third criterion has to do with the asymptotic variance of the ML estimator of the transformed shape parameter ϕ , namely, it should vary as little as possible for “moderate” values of ϕ that correspond to the interval $\xi \in [-0.3, 0.3]$. This ensures that additive effects in ϕ have the same “impact” on the model, which is crucial when covariates are involved in a linear way. The forth criterion states that ϕ should be approximately equal to ξ for values

of ξ around zero, which facilitates interpretation. A transformation that matches these criteria reasonably well is given by

$$\phi = h(\xi) = a_\phi + b_\phi \log[-\log\{1 - (\xi + 1/2)^{c_\phi}\}]$$

where $c_\phi = 0.8$,

$$b_\phi = -c_\phi^{-1} \log\{1 - (1/2)^{c_\phi}\} \{1 - (1/2)^{c_\phi}\} 2^{c_\phi-1} = 0.39563,$$

$$a_\phi = -b_\phi \log[-\log\{1 - (1/2)^{c_\phi}\}] = 0.062376.$$

The constants a_ϕ and b_ϕ stem from the fourth criterion, that is,

$$\left. \frac{dh(\xi)}{d\xi} \right|_{\xi=0} = h'(0) = 1, \quad h(0) = 0,$$

meaning that if ξ is close to zero then $\phi = h(\xi) \approx \xi$. Furthermore, the inverse of the transformation is

$$\xi = h^{-1}(\phi) = g(\phi) = \left[1 - \exp \left\{ - \exp \left(\frac{\phi - a_\phi}{b_\phi} \right) \right\} \right]^{1/c_\phi} - \frac{1}{2}. \quad (1)$$

The transformation from ξ to ϕ via $h(\cdot)$ is shown in Figure 1.

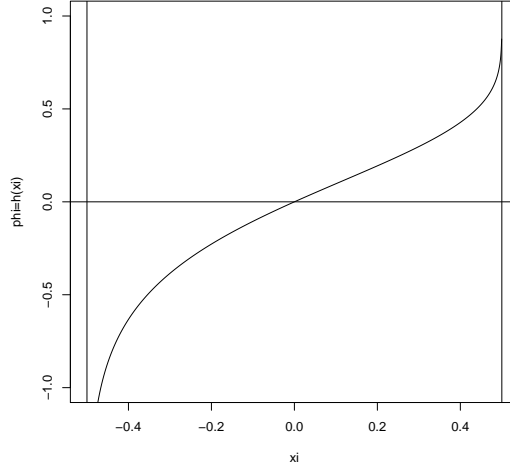


Figure 1: The transformation for the shape parameter, $\phi = h(\xi)$.

1.3 A prior for the shape parameter

As mentioned above, we assume that the shape parameter ξ lies in the interval $(-0.5, 0.5)$. We propose using a prior density that reflects our primary beliefs about ξ in addition to the Gaussian prior density at the latent level. Raw ML estimates of ξ at each site in the UK flood dataset are used to get an idea about the variability in ξ . We believe that ξ is most likely within $[-0.3, 0.3]$

and that it is unlikely to be in the intervals $(-0.5, -0.4)$ and $(0.4, 0.5)$. These prior beliefs can be presented with a shifted beta density with parameters $\alpha = 4$ and $\beta = 4$, see Figure 2. Note that this prior density is similar to (but slightly different from) the prior proposed by Martins and Stedinger (2000).

The prior density for ϕ can be found from the prior density for ξ and the relationship between ϕ and ξ . It is given by

$$\begin{aligned} \pi(\phi) = & \frac{\Gamma(\alpha + \beta)}{\Gamma(\alpha)\Gamma(\beta)b_\phi c_\phi} (g(\phi) + 1/2)^{\alpha - c_\phi} (1/2 - g(\phi))^{\beta - 1} \\ & \times \exp \left\{ \left(\frac{\phi - a_\phi}{b_\phi} \right) - \exp \left(\frac{\phi - a_\phi}{b_\phi} \right) \right\}, \end{aligned} \quad (2)$$

where $\Gamma(\cdot)$ denotes the gamma function. The right panel of Figure 2 shows the prior density for ϕ .

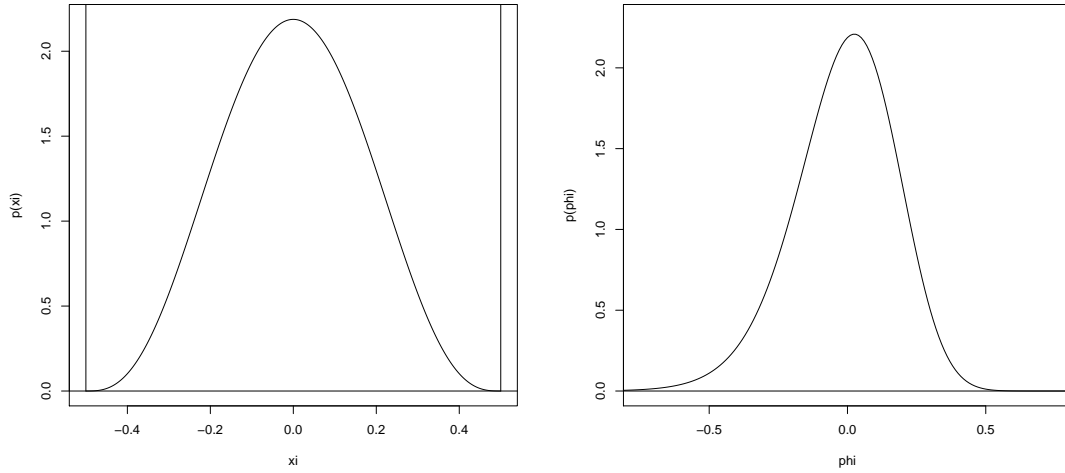


Figure 2: The prior density for the shape parameter ξ (left panel). The prior density for the transformed shape parameter ϕ (right panel).

1.4 The asymptotic standard deviation of the shape parameter

When $\xi > -1/2$, the asymptotic efficiency and asymptotic normality of $(\hat{\mu}, \hat{\sigma}, \hat{\xi})^\top$, the ML estimator for $(\mu, \sigma, \xi)^\top$ in the GEV distribution, hold (Smith, 1985). This property can be expressed as

$$\sqrt{n}\{(\hat{\mu}, \hat{\sigma}, \hat{\xi})^\top - (\mu, \sigma, \xi)^\top\} \rightarrow N(0, I^{-1}(\mu, \sigma, \xi)), \quad \text{as } n \rightarrow \infty,$$

where $I(\mu, \sigma, \xi)$ is the Fisher information stemming from the GEV distribution, see p.169 in Beirlant et al. (2004). The asymptotic standard deviation of ξ (i.e., the square root of the $(3, 3)$ -entry of the matrix $I^{-1}(\mu, \sigma, \xi)$) is shown in the left panel of Figure 3.

In our statistical model presented below, the following transformation of the GEV parameters is used:

$$\psi = \log(\mu), \quad \tau = \log(\sigma/\mu), \quad \text{and} \quad \phi = h(\xi).$$

The asymptotic distribution for the ML estimator $(\hat{\psi}, \hat{\tau}, \hat{\phi})$ is therefore

$$\sqrt{n}\{(\hat{\psi}, \hat{\tau}, \hat{\phi})^\top - (\psi, \tau, \phi)^\top\} \rightarrow N(0, \{D^\top I(\mu, \sigma, \xi) D\}^{-1}),$$

where

$$D = \begin{bmatrix} \exp(\psi) & 0 & 0 \\ \exp(\psi + \tau) & \exp(\psi + \tau) & 0 \\ 0 & 0 & \frac{dg(\phi)}{d\phi} \end{bmatrix}.$$

The asymptotic standard deviation of ϕ is shown in the right panel of Figure 3. We can see that the third criterion is met, that is, the asymptotic variance of the ML for ϕ does not vary much in the interval $[-0.3, 0.3]$.

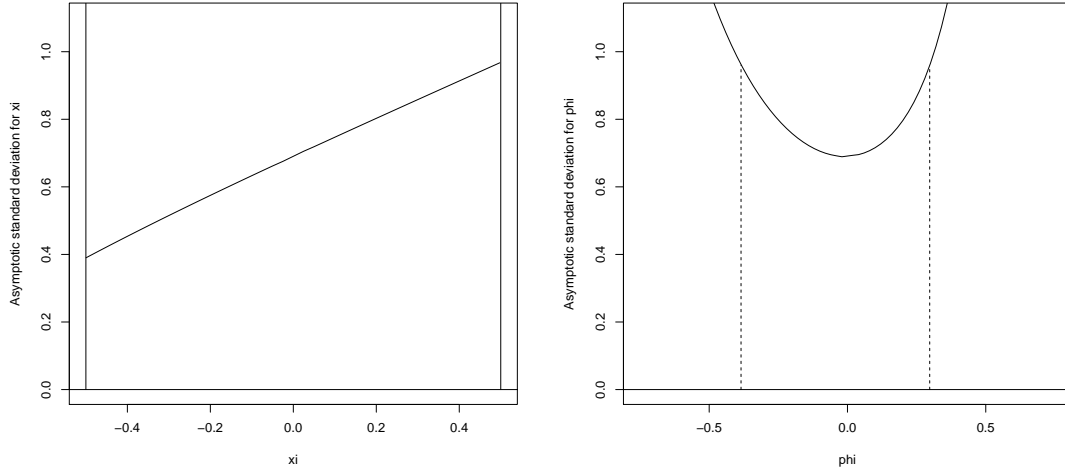


Figure 3: Left panel: The asymptotic standard deviation of ξ . Right panel: The asymptotic standard deviation of ϕ . The vertical dashed lines show the two values of ϕ that correspond to $\xi = -0.3$ and $\xi = 0.3$, respectively. The asymptotic standard deviation of ϕ at these two values is nearly the same.

1.5 Statistical model

Here y_{it} denotes the observed extreme value at site i and time t . The data are assumed to follow the GEV distribution with location parameter μ_i , scale parameter σ_i and shape parameter ξ_i , i.e.,

$$y_{it} \sim \text{GEV}(\mu_i, \sigma_i, \xi_i), \quad \mu_i, \sigma_i \in \mathbb{R}_+, \quad \xi_i \in (-0.5, 0.5),$$

where $i \in \{1, \dots, J\}$ and $t \in \{1, \dots, T\}$, J is the number of stations and T is the number of time points. The data density for the data at site i , $\mathbf{y}_i = (y_{i1}, \dots, y_{iT})^\top$, is given by

$$\pi(\mathbf{y}_i | \mu_i, \sigma_i, \xi_i) = \prod_{t=1}^T \frac{1}{\sigma_i} \left\{ 1 + \xi \left(\frac{y_{it} - \mu_i}{\sigma_i} \right) \right\}^{-1/\xi_i - 1} \exp \left[- \left\{ 1 + \xi_i \left(\frac{y_{it} - \mu_i}{\sigma_i} \right) \right\}^{-1/\xi_i} \right] \quad (3)$$

for $1 + \xi_i(y_{it} - \mu_i)/\sigma_i > 0$. The parameters μ_i , σ_i and ξ_i are transformed to $\psi_i = \log(\mu_i)$, $\tau_i = \log(\sigma_i/\mu_i)$ and $\phi_i = h(\xi_i)$, so $\psi_i, \tau_i, \phi_i \in \mathbb{R}$. The data density in terms of ψ_i , τ_i and ϕ_i is

$$\begin{aligned} \pi(\mathbf{y}_i | \psi_i, \tau_i, \phi_i) &= \prod_{t=1}^T \frac{1}{\exp(\tau_i + \psi_i)} \left[1 + g(\phi_i) \left\{ \frac{y_{it} - \exp(\psi_i)}{\exp(\tau_i + \psi_i)} \right\} \right]^{-1/g(\phi_i) - 1} \\ &\times \prod_{t=1}^T \exp \left(- \left[1 + g(\phi_i) \left\{ \frac{y_{it} - \exp(\psi_i)}{\exp(\tau_i + \psi_i)} \right\} \right]^{-1/g(\phi_i)} \right) \end{aligned} \quad (4)$$

for $1 + g(\phi)\{y_{it} - \exp(\psi_i)\}/\exp(\tau_i + \psi_i) > 0$, where $g(\phi) = h^{-1}(\phi)$, and g is given in (1).

The parameters are collected into the vectors $\boldsymbol{\psi} = (\psi_1, \dots, \psi_J)^\top$, $\boldsymbol{\tau} = (\tau_1, \dots, \tau_J)^\top$ and $\boldsymbol{\phi} = (\phi_1, \dots, \phi_J)^\top$. The latent level consists of three linear predictors for $\boldsymbol{\psi}$, $\boldsymbol{\tau}$ and $\boldsymbol{\phi}$ of the form

$$\begin{aligned} \boldsymbol{\psi} &= X_\psi \boldsymbol{\beta}_\psi + A \mathbf{u}_\psi + \boldsymbol{\epsilon}_\psi, \\ \boldsymbol{\tau} &= X_\tau \boldsymbol{\beta}_\tau + A \mathbf{u}_\tau + \boldsymbol{\epsilon}_\tau, \\ \boldsymbol{\phi} &= X_\phi \boldsymbol{\beta}_\phi + \boldsymbol{\epsilon}_\phi, \end{aligned} \quad (5)$$

where \mathbf{u}_ψ and \mathbf{u}_τ are spatial terms modeled according to the SPDE approach of Lindgren et al. (2011), with hyperparameters $s_l, \rho_l, l = \psi, \tau$. The first of these hyperparameters is the marginal standard deviation of \mathbf{u}_l , the second one is the range parameter of \mathbf{u}_l . The term $\boldsymbol{\epsilon}_l$ denotes an unstructured term with a standard deviation σ_{ϵ_l} , $l = \psi, \tau, \phi$. The matrices X_ψ , X_τ and X_ϕ are such that their first column is a vector of ones and the other columns may contain hydrological, meteorological and geographical covariates. The vectors $\boldsymbol{\beta}_\psi$, $\boldsymbol{\beta}_\tau$ and $\boldsymbol{\beta}_\phi$ are the corresponding parameters.

1.6 Approximate Bayesian inference

The inference for the above model described in Section 1.5 is performed in two steps, with correct uncertainty propagation from the first to the second step. Precisely, the maximum likelihood estimates are computed first at each site separately, and then modeled subsequently using a latent Gaussian model with a trivariate link function where all the elements of the link function are identity links, namely, the Gaussian–Gaussian model described in Section 4.1 of the main paper.

Let $\boldsymbol{\omega}_i = (\mu_i, \sigma_i, \xi_i)^\top$ and let $f : \mathbb{R}_+^2 \times (-0.5, 0.5) \rightarrow \mathbb{R}^3$ be a trivariate link function such that $g(x_1, x_2, x_3) = (\log(x_1), \log(x_2/x_1), h(x_3))^\top$ and

$$f^{-1}(u_1, u_2, u_3) = (\exp(u_1), \exp(u_1 + u_2), h^{-1}(u_3))^\top$$

Let

$$\boldsymbol{\eta}_i := (\psi_i, \tau_i, \phi_i)^\top = g(\boldsymbol{\omega}_i) = (\log(\mu_i), \log(\sigma_i/\mu_i), h(\xi_i))^\top.$$

Now define the generalized likelihood function $L(\boldsymbol{\eta}_i) = \pi(\mathbf{y}_i|\psi_i, \tau_i, \phi_i)\pi(\phi_i)$ where $\pi(\mathbf{y}_i|\psi_i, \tau_i, \phi_i)$ is the data density for site i given by (4) and $\pi(\phi_i)$ is the prior density for ϕ_i , see (2).

In the first step, we compute $\hat{\boldsymbol{\eta}}_i := (\hat{\psi}_i, \hat{\tau}_i, \hat{\phi}_i)^\top$, which is the mode of $L(\boldsymbol{\eta}_i)$, and

$$H_{\eta_i} = \nabla^2 \log(L(\boldsymbol{\eta}_i|\mathbf{y}_i))|_{\eta_i=\hat{\eta}_i}$$

which is the Hessian matrix corresponding to the logarithm of the generalized likelihood evaluated at the mode $\hat{\boldsymbol{\eta}}_i$. The terms $\hat{\boldsymbol{\eta}}_i$ and H_{η_i} are computed at each site independently from the other sites. Furthermore, the observed information matrix corresponding to the generalized likelihood is defined as $\mathcal{I}_{\eta y_i} = -H_{\eta_i}$.

In the second step, instead of using \mathbf{y}_i as the data, we now treat $\hat{\boldsymbol{\eta}}_i = (\hat{\psi}_i, \hat{\tau}_i, \hat{\phi}_i)^\top$ as the data for site i . The generalized likelihood function for $\boldsymbol{\eta}_i$ can then be approximated by a Gaussian likelihood as

$$L(\boldsymbol{\eta}_i) = \pi(\mathbf{y}_i|\boldsymbol{\eta}_i)\pi(\phi_i) \approx c_i \hat{L}(\boldsymbol{\eta}_i) = c_i \pi(\boldsymbol{\eta}_i|\hat{\boldsymbol{\eta}}_i) = c_i \mathcal{N}(\boldsymbol{\eta}_i|\hat{\boldsymbol{\eta}}_i, \mathcal{I}_{\eta y_i}^{-1}),$$

where c_i is a constant independent of $\boldsymbol{\eta}_i$.

Now let $\boldsymbol{\eta} = (\boldsymbol{\psi}^\top, \boldsymbol{\tau}^\top, \boldsymbol{\phi}^\top)^\top$ with $\boldsymbol{\psi}$, $\boldsymbol{\tau}$ and $\boldsymbol{\phi}$ as before. Then, the generalized likelihood function of $\boldsymbol{\eta}$, $L(\boldsymbol{\eta})$, may be approximated with $\hat{L}(\boldsymbol{\eta})$, that is

$$L(\boldsymbol{\eta}) = \prod_{i=1}^J L(\boldsymbol{\eta}_i) \approx c \hat{L}(\boldsymbol{\eta}) = \prod_{i=1}^J c_i \hat{L}(\boldsymbol{\eta}_i) = c \mathcal{N}(\boldsymbol{\eta}|\hat{\boldsymbol{\eta}}, Q_{\eta y}^{-1}),$$

where $\hat{\boldsymbol{\eta}} = (\hat{\boldsymbol{\psi}}^\top, \hat{\boldsymbol{\tau}}^\top, \hat{\boldsymbol{\phi}}^\top)^\top$ and $c = \prod_{i=1}^J c_i$. Define $\hat{\boldsymbol{\eta}}^* := (\hat{\psi}_1, \hat{\tau}_1, \hat{\phi}_1, \dots, \hat{\psi}_J, \hat{\tau}_J, \hat{\phi}_J)^\top$ as a rearrangement of $\hat{\boldsymbol{\eta}}$ then the block-diagonal matrix

$$(Q_{\eta y}^*)^{-1} = \text{bdiag}(\mathcal{I}_{\eta y_1}^{-1}, \dots, \mathcal{I}_{\eta y_J}^{-1})$$

is known, and it is possible to rearrange $(Q_{\eta y}^*)^{-1}$ accordingly to get $Q_{\eta y}^{-1}$.

In the pseudo Gaussian–Gaussian model that is used for inference, $\hat{\boldsymbol{\eta}}$ is taken as the data and $Q_{\eta y}^{-1}$ as fixed. The approximate data distribution is thus

$$\pi(\hat{\boldsymbol{\eta}}|\boldsymbol{\eta}, \boldsymbol{\nu}, \boldsymbol{\theta}) = \mathcal{N}(\hat{\boldsymbol{\eta}}|\boldsymbol{\eta}, Q_{\eta y}^{-1}),$$

where $\boldsymbol{\nu}$ are all unknown parameters that are assigned a Gaussian prior distribution and $\boldsymbol{\theta}$ are all unknown hyperparameters. The vectors \mathbf{x} , $\boldsymbol{\eta}$, $\boldsymbol{\nu}$ and $\boldsymbol{\theta}$ are such that

$$\mathbf{x}^\top = (\boldsymbol{\eta}^\top, \boldsymbol{\nu}^\top), \quad \boldsymbol{\eta}^\top = (\boldsymbol{\psi}^\top, \boldsymbol{\tau}^\top, \boldsymbol{\phi}^\top), \quad \boldsymbol{\nu}^\top = (\boldsymbol{\beta}_\psi^\top, \mathbf{u}_\psi^\top, \boldsymbol{\beta}_\tau^\top, \mathbf{u}_\tau^\top, \boldsymbol{\beta}_\phi^\top)$$

and

$$\boldsymbol{\theta} = (\theta_1, \dots, \theta_7)^\top = (\sigma_{\epsilon\psi}, s_\psi, \rho_\psi, \sigma_{\epsilon\tau}, s_\tau, \rho_\tau, \sigma_{\epsilon\phi})^\top.$$

Posterior inference for $\boldsymbol{\eta}$, $\boldsymbol{\nu}$ and $\boldsymbol{\theta}$ is based on the above Gaussian approximation for $\hat{\boldsymbol{\eta}}$ conditional on $\boldsymbol{\eta}$, $\boldsymbol{\nu}$ and $\boldsymbol{\theta}$. This pseudo Gaussian–Gaussian model can be written hierarchically as

$$\begin{aligned} \pi(\hat{\boldsymbol{\eta}}|\boldsymbol{\eta}, Q_{\eta y}, \boldsymbol{\theta}) &= \mathcal{N}(\hat{\boldsymbol{\eta}}|\boldsymbol{\eta}, Q_{\eta y}^{-1}), \\ \pi(\boldsymbol{\eta}|\boldsymbol{\nu}, \boldsymbol{\theta}) &= \mathcal{N}(\boldsymbol{\eta}|\mathbf{Z}\boldsymbol{\nu}, Q_\epsilon^{-1}), \\ \pi(\boldsymbol{\nu}|\boldsymbol{\theta}) &= \mathcal{N}(\boldsymbol{\nu}|\boldsymbol{\mu}_\nu, Q_\nu^{-1}) \end{aligned}$$

and $\pi(\boldsymbol{\theta})$ is the prior density for $\boldsymbol{\theta}$. The posterior density for this model is thus given by

$$\begin{aligned}\pi(\boldsymbol{\eta}, \boldsymbol{\nu}, \boldsymbol{\theta} | \hat{\boldsymbol{\eta}}) &\propto \pi(\boldsymbol{\theta}) \pi(\boldsymbol{\eta} | \boldsymbol{\nu}, \boldsymbol{\theta}) \pi(\boldsymbol{\nu} | \boldsymbol{\theta}) \pi(\hat{\boldsymbol{\eta}} | \boldsymbol{\eta}, Q_{\eta y}, \boldsymbol{\theta}) \\ &\propto \pi(\boldsymbol{\theta}) \pi(\boldsymbol{\eta} | \boldsymbol{\nu}, \boldsymbol{\theta}) \pi(\boldsymbol{\nu} | \boldsymbol{\theta}) \mathcal{N}(\hat{\boldsymbol{\eta}} | \boldsymbol{\eta}, Q_{\eta y}^{-1}) \\ &\propto \pi(\boldsymbol{\theta}) \mathcal{N}(\boldsymbol{\eta} | Z\boldsymbol{\nu}, Q_{\epsilon}^{-1}) \mathcal{N}(\boldsymbol{\nu} | \boldsymbol{\mu}_{\nu}, Q_{\nu}^{-1}) \mathcal{N}(\hat{\boldsymbol{\eta}} | \boldsymbol{\eta}, Q_{\eta y}^{-1}),\end{aligned}$$

where

$$Q_{\epsilon} = \text{bdiag}(Q_{\epsilon,1}, Q_{\epsilon,2}, Q_{\epsilon,3}) = \text{bdiag}(\sigma_{\epsilon\psi}^{-2}I, \sigma_{\epsilon\tau}^{-2}I, \sigma_{\epsilon\phi}^{-2}I),$$

$$Q_{\nu}^{-1} = \text{bdiag}(Q_{\psi}, Q_{\tau}, Q_{\phi}),$$

and Z is based on X_{ψ} , A_{ψ} , X_{τ} , A_{τ} and X_{ϕ} , namely,

$$Z = \begin{pmatrix} X_{\psi} & A_{\psi} & \cdot & \cdot & \cdot \\ \cdot & \cdot & X_{\tau} & A_{\tau} & \cdot \\ \cdot & \cdot & \cdot & \cdot & X_{\phi} \end{pmatrix},$$

where the dots denote zero entries.

1.7 Approximation accuracy

In this subsection, we focus on the Gaussian approximation to the likelihood function, $L(\boldsymbol{\eta}_i)$, while other aspects of the inference scheme for $\boldsymbol{\eta}$, $\boldsymbol{\nu}$ and $\boldsymbol{\theta}$ are not considered. The normalized likelihood is treated as a probability density and the marginal probability densities of ψ , τ and ϕ are derived with numerical integration. Figures 4 to 8 show the marginal normalized likelihood densities of ψ , τ and ϕ along with the marginal densities of the trivariate Gaussian density that was used to approximate the likelihood in the case of $T = 20, 50, 80$ time replicates when the true value of ξ was 0.475, 0.25, 0.0, -0.25 and -0.475, and $\psi = 3$ and $\tau = -1$. In the case when the true value of the shape parameter is $\xi = 0.475$, the three datasets ($T = 20, 50, 80$) were select such that the unconstrained ML estimates for ξ were larger than 0.5, $\hat{\xi} > 0.5$, and in the case when the true value is $\xi = -0.475$, the three dataset were select such that $\hat{\xi} < -0.5$. These six datasets were select in this way to test the approximation when the unconstrained likelihood function as a function of ξ has its maximum over $\xi > 0.5$ or over $\xi < -0.5$.

The Gaussian approximation is reasonably good in the case of ψ and ϕ when $T = 50$ and $T = 80$. When $T = 20$, the skewness in the marginal normalized likelihood densities of ψ and ϕ is apparent. The results show that the skewness in the marginal normalized likelihood densities for ψ and ϕ reduces dramatically as the sample size T increases. Furthermore, when $\xi = 0.475$ and $\hat{\xi} > 0.5$, the Gaussian approximation with respect to ϕ is convincing and in the case $\xi = -0.475$ and $\hat{\xi} < -0.5$ it is reasonably good. This shows that the joint effect of the transformation $\phi = h(\xi)$ and the penalizing prior for ϕ stabilizes the marginal normalized likelihood density ϕ . In the case of τ the Gaussian approximation is acceptable in the case of $T = 80$, however, the Gaussian approximation is slightly shifted to the left of the marginal normalized likelihood density. In the case of τ when $T = 20$, this shift is quite substantial, and when $T = 50$ the shift is apparent. When T is too small, the three-dimensional likelihood function is not close enough to the elliptically shaped Gaussian approximation, which results in too much probability mass concentrated on the right of the mode of τ compared to the mass on the left of the mode of τ . Therefore, the value of τ at the mode of the likelihood for $(\psi, \tau, \phi)^T$ is slightly smaller than the value of τ at the mode of the marginal normalized likelihood density of τ .

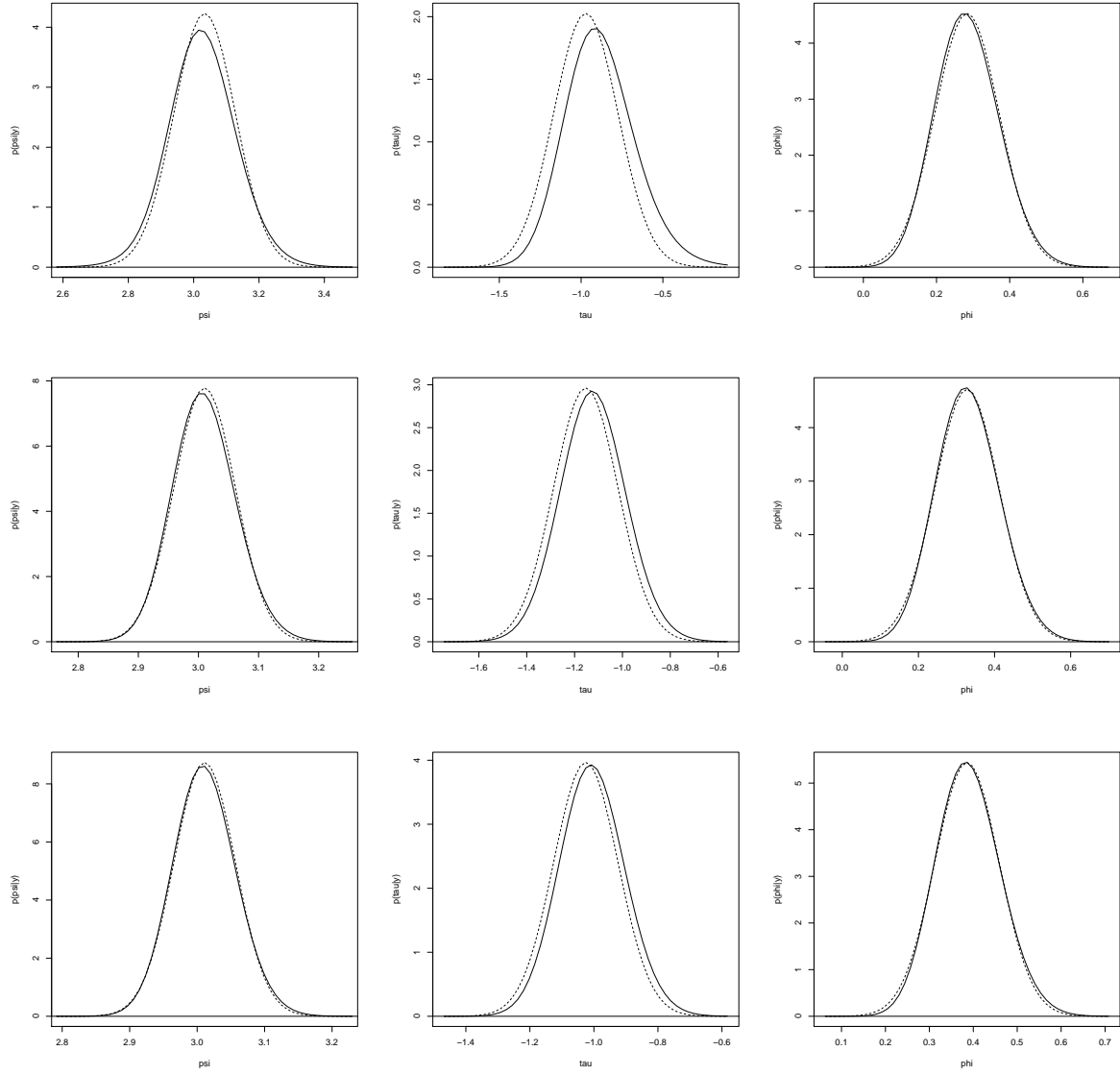


Figure 4: The marginal normalized likelihood densities (solid lines) of ψ (left column of panel), τ (middle column of panel) and ϕ (right column of panel), along with the marginal Gaussian densities based on the Gaussian approximation of the likelihood function (dashed lines) when $\xi = 0.475$ and $\hat{\xi} > 0.5$. The top, middle and bottom row panels show the results for $T = 20, 50, 80$, respectively.

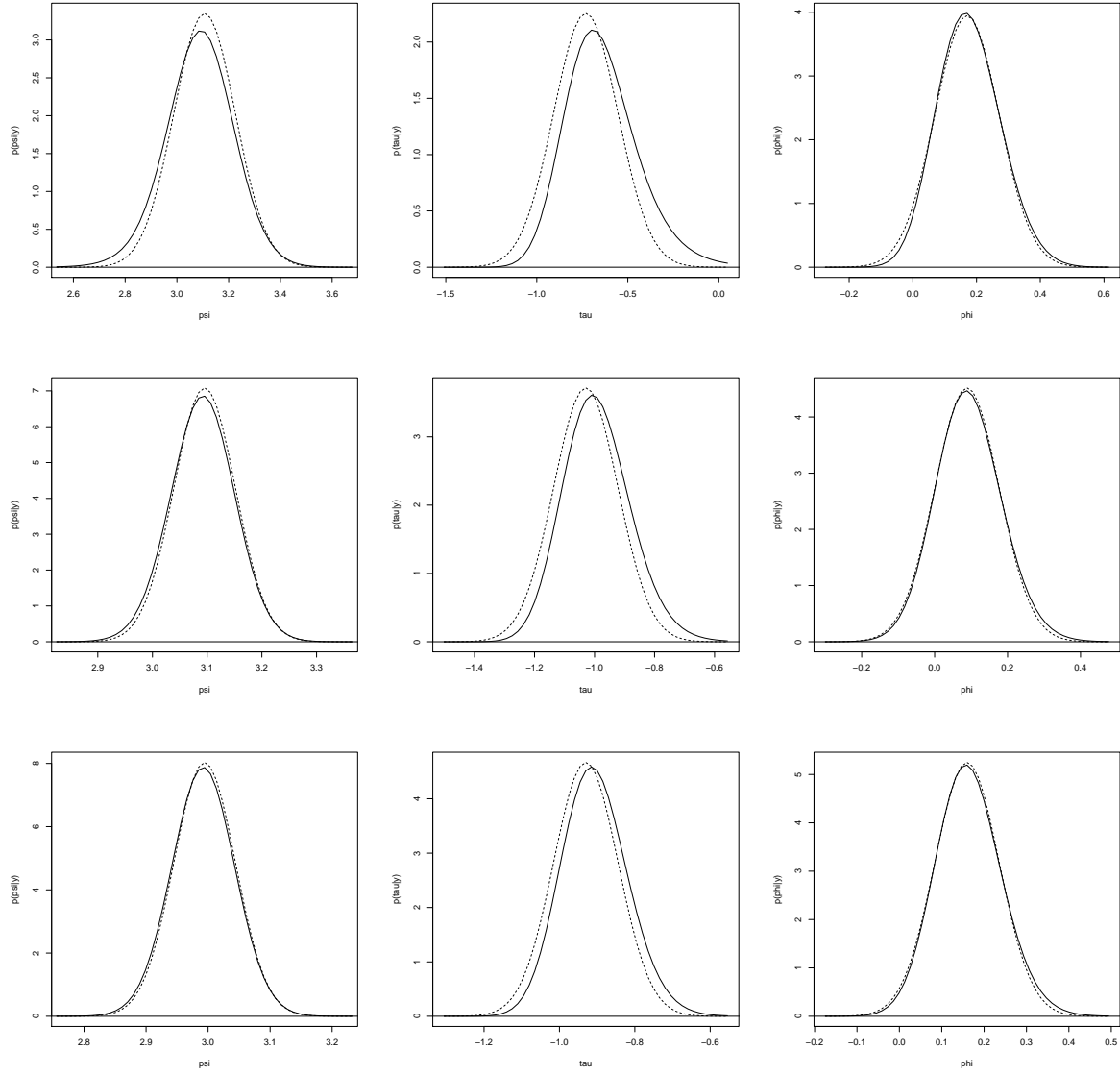


Figure 5: The marginal normalized likelihood densities (solid lines) of ψ (left column of panel), τ (middle column of panel) and ϕ (right column of panel), along with the marginal Gaussian densities based on the Gaussian approximation of the likelihood function (dashed lines) when $\xi = 0.25$. The top, middle and bottom row panels show the results for $T = 20, 50, 80$, respectively.

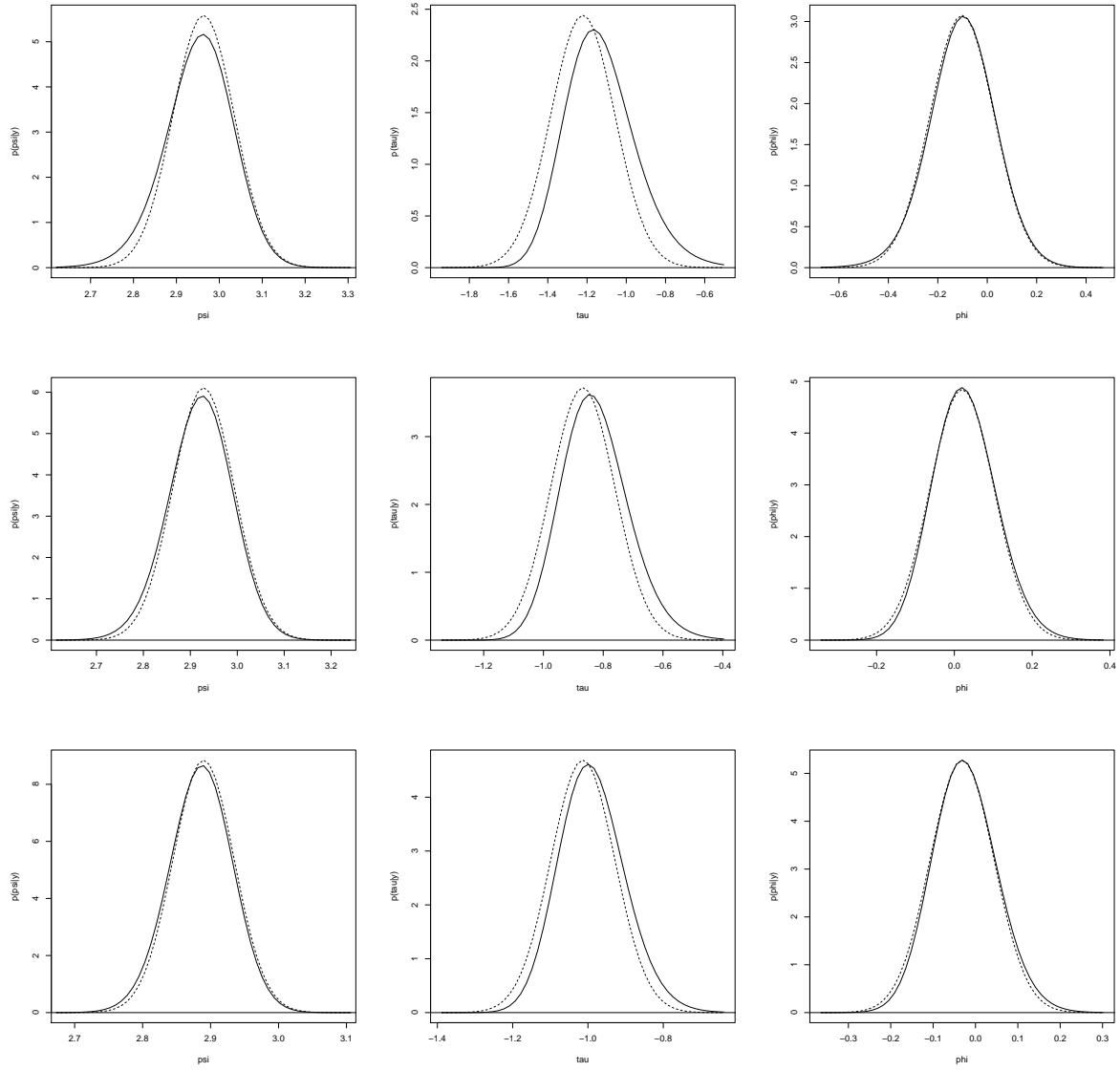


Figure 6: The marginal normalized likelihood densities (solid lines) of ψ (left column of panel), τ (middle column of panel) and ϕ (right column of panel), along with the marginal Gaussian densities based on the Gaussian approximation of the likelihood function (dashed lines) when $\xi = 0.0$. The top, middle and bottom row panels show the results for $T = 20, 50, 80$, respectively.

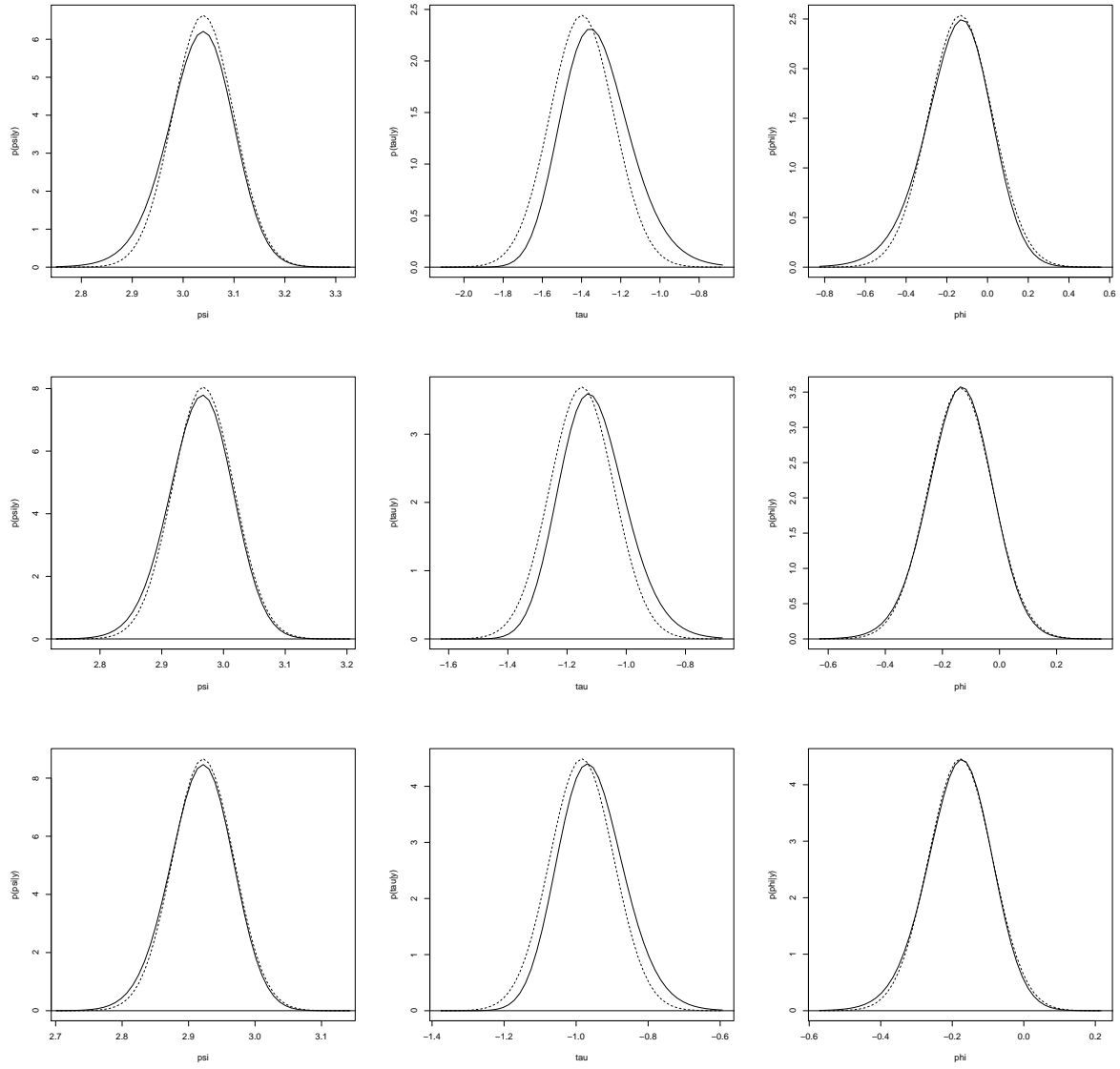


Figure 7: The marginal normalized likelihood densities (solid lines) of ψ (left column of panel), τ (middle column of panel) and ϕ (right column of panel), along with the marginal Gaussian densities based on the Gaussian approximation of the likelihood function (dashed lines) when $\xi = -0.25$. The top, middle and bottom row panels show the results for $T = 20, 50, 80$, respectively.

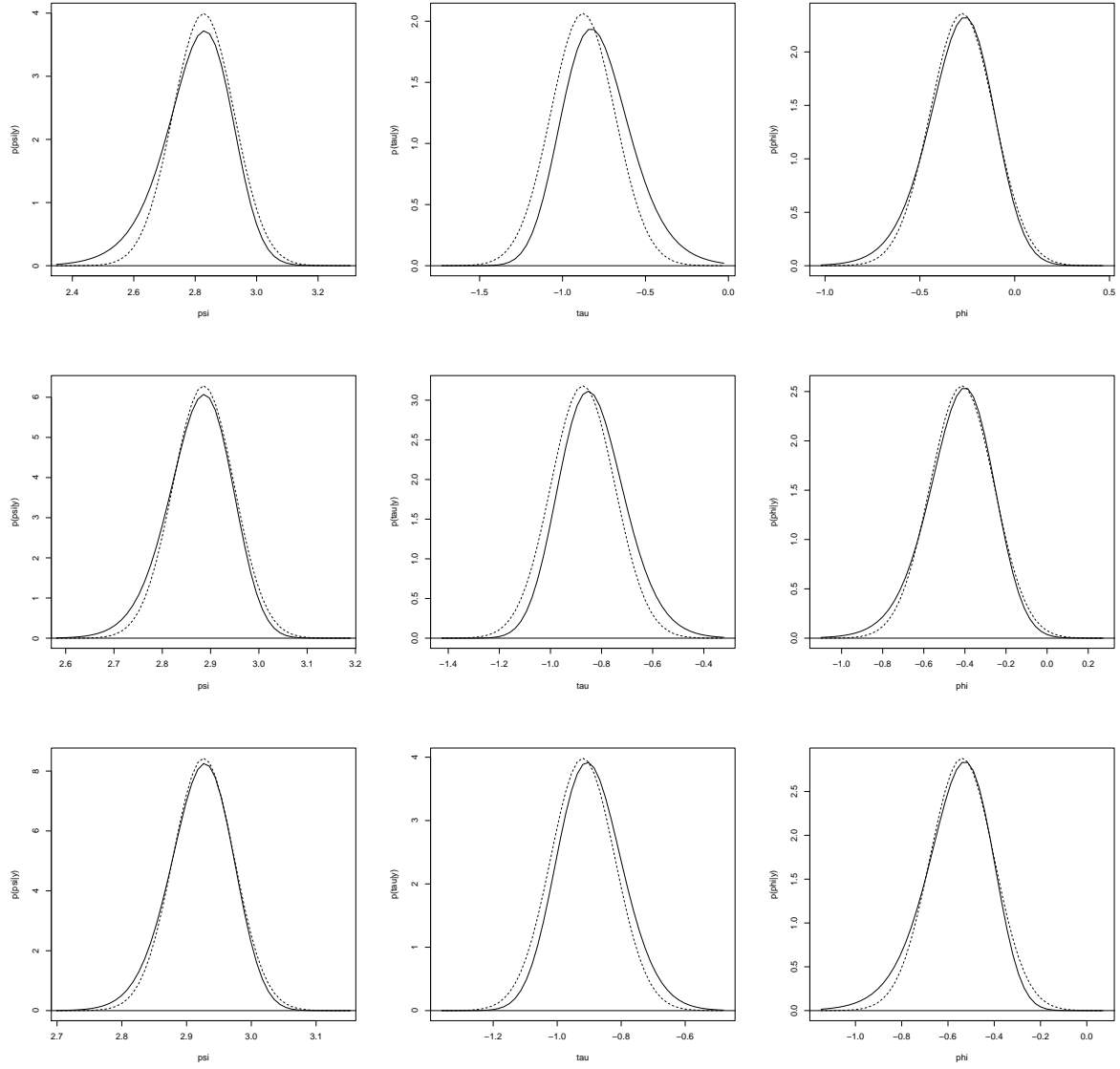


Figure 8: The marginal normalized likelihood densities (solid lines) of ψ (left column of panel), τ (middle column of panel) and ϕ (right column of panel), along with the marginal Gaussian densities based on the Gaussian approximation of the likelihood function (dashed lines) when $\xi = -0.475$ and $\hat{\xi} < -0.5$. The top, middle and bottom row panels show the results for $T = 20, 50, 80$, respectively.

2 Preliminary data analysis

2.1 ML estimates of the GEV parameters

Figure 9 shows the relationship between the ML estimates of the scale parameter, σ , and the location parameter, μ , on the log-scale. There is a clear positive relationship between them, however by using the transformation, $\tau_i = \log(\sigma_i/\mu_i)$, for all stations i , one can see from Figure 10 that this transformation is such that it is weakly correlated with the location parameter on the logarithmic scale.

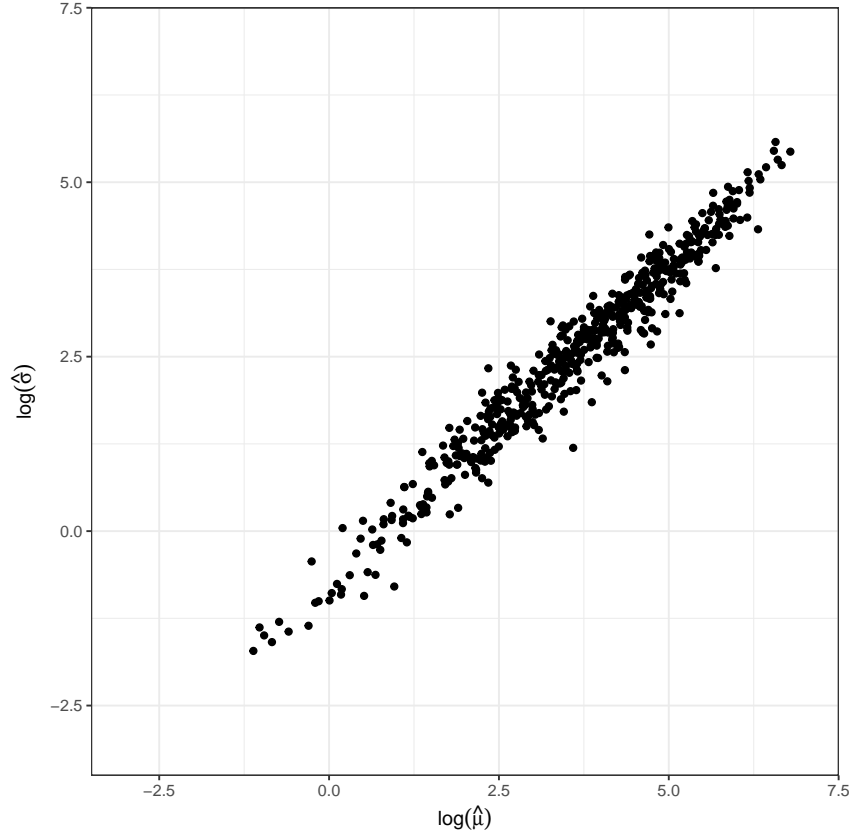


Figure 9: The ML estimates of the log-scale parameter, $\log(\hat{\sigma})$, from all the observational sites, as a function of the ML estimates of the log-location parameter, $\log(\hat{\mu})$, from the corresponding observational sites.

The data contain spatial information and this information can potentially be useful. In order to explore the spatial correlation in the data two models were proposed, one for the sample median and one for the sample IQR, using informative catchment descriptors. The models are

$$\begin{aligned} \log(\text{median}_i) = & \beta_0 + \beta_1 \log(\text{Area}_i) + \beta_2 \log(\text{SAAR}_i) + \beta_3 \log(\text{FARL}_i) \\ & + \beta_4 \log(\text{BFIHOST}_i) + \beta_5 \log(\text{URBEXT}+1_i) \\ & + \beta_6 \log(\text{PROPWET}_i) \end{aligned} \quad (6)$$

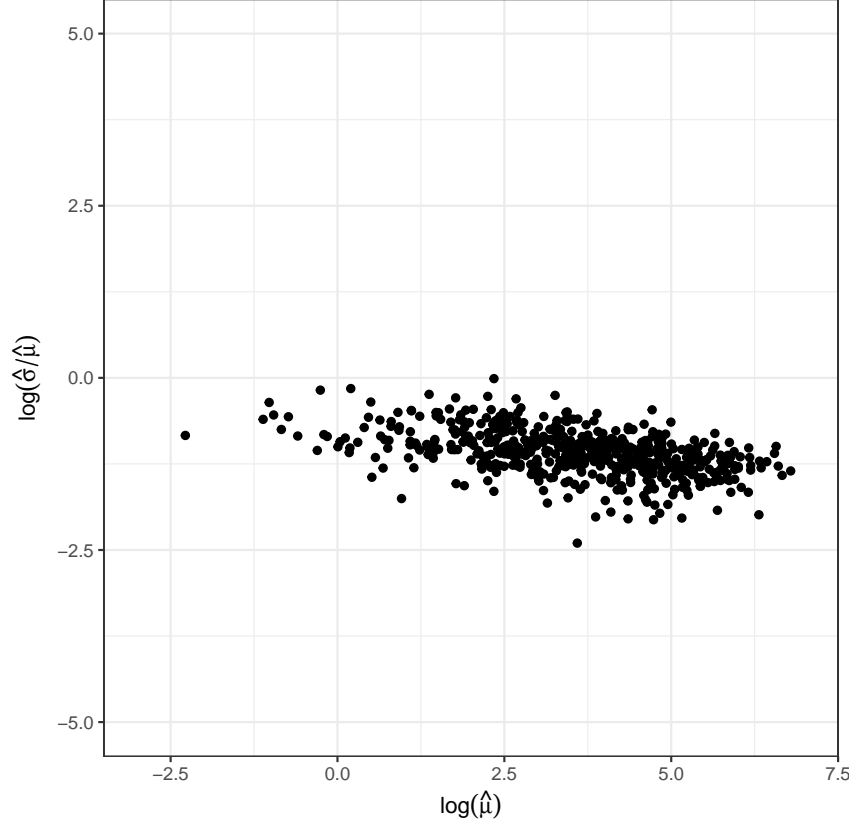


Figure 10: The ML estimates of the log-ratio of the scale and location parameter, $\log(\hat{\sigma}/\hat{\mu})$, from all the observational sites, as a function of the ML estimates of the log-location parameter, $\log(\hat{\mu})$, from the corresponding observational sites.

and

$$\begin{aligned} \log(\text{IQR}_i/\text{median}_i) = & \alpha_0 + \alpha_1 \log(\text{Area}_i) + \alpha_2 \log(\text{SAAR}_i) + \alpha_3 \log(\text{FARL}_i) \\ & + \alpha_4 \log(\text{FPEXT}_i) + \alpha_5 \log(\text{URBEXT}+1_i) \\ & + \alpha_6 \log(\text{PROPWET}_i) + \alpha_7 \log(\text{ALTBAR}_i). \end{aligned} \quad (7)$$

Figure 11 shows variograms for the residuals of the models in (6) and (7). The variograms suggest that there is still some spatial correlation in the logarithm of the sample median and the logarithm of the sample IQR over the sample median that is not explained by the catchment descriptors (covariates). This is a strong indication of using spatial model components for $\log(\mu)$ and $\log(\sigma/\tau)$. Moreover, the discontinuity of the variogram at the origin suggests that an unstructured “nugget effect” should also be included.

The generalized maximum likelihood estimates of the parameters GEV parameters, μ , σ and ξ , were computed at each of the observational the sites along with the generalized ML estimates of the transformed parameters, ψ , τ and ϕ , i.e., the generalized likelihoods with the beta prior for ξ and the transformed the beta prior for ϕ were maximized. Histograms of these estimates are shown in Figure 12.

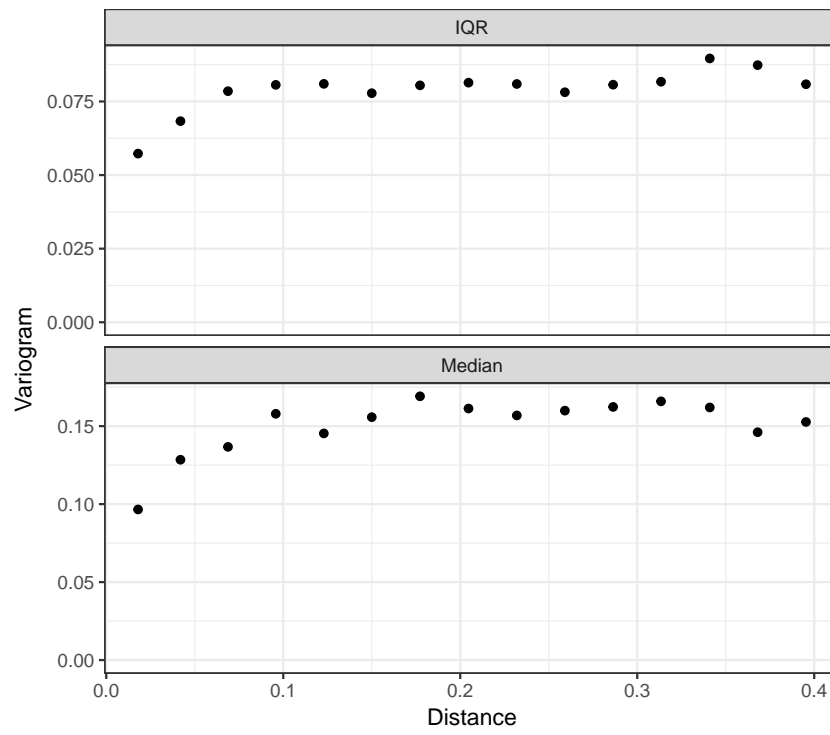


Figure 11: A variogram for the residuals of Models 6 and 7.

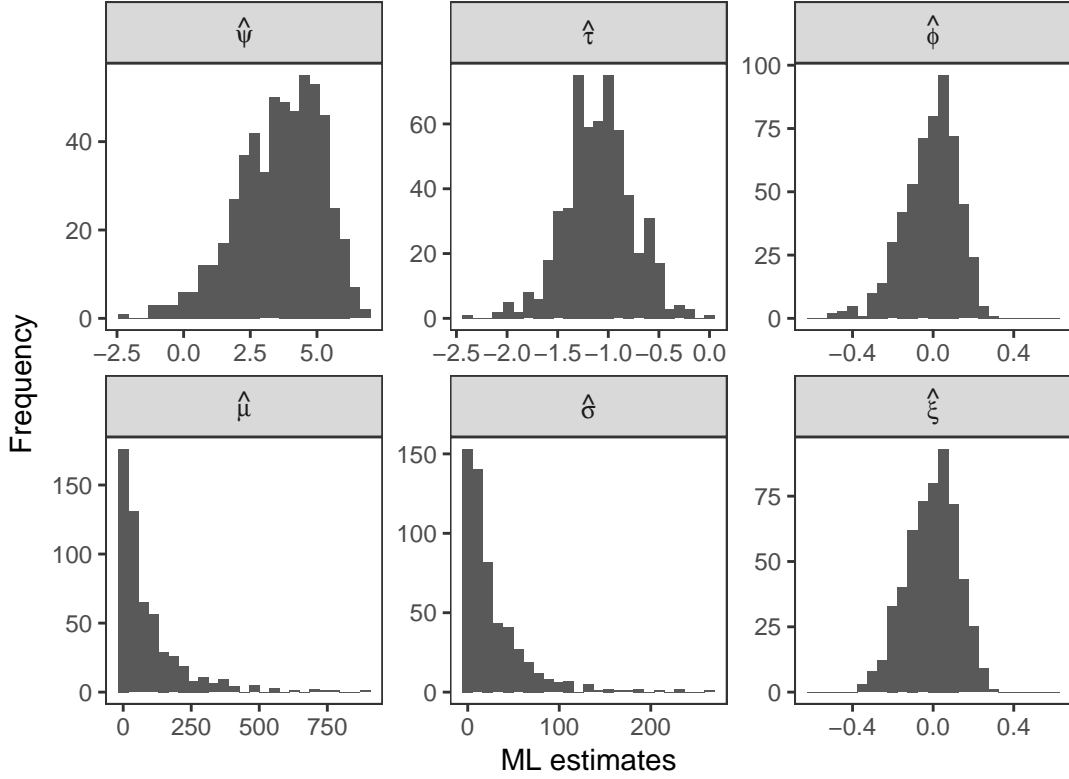


Figure 12: Histograms of the generalized ML estimates of the GEV parameters, μ , σ and ξ , from the observational the sites (bottom panel) along with the generalized ML estimates of the transformed parameters (top panel), ψ , τ and ϕ .

2.2 Goodness-of-fit

To test the goodness-of-fit of the GEV model to the annual maximum flow at each station, the Anderson-Darling test from Stephens (1974) was used. The p -values of the Anderson-Darling test, using the ML estimates of μ , σ and ξ (no beta prior density involved) as parameters in the GEV density, are presented in Figure 13. The Anderson-Darling test is a classical statistics test, and is used here to give an idea about how well the GEV density, using the ML estimates as parameters, fits the data. Here the null hypothesis of the Anderson-Darling test states that the data follow the GEV distribution. This means that a p -value close to zero indicates that the data does not follow the specified distribution. The GEV density fits the data well according to Figure 13 since only five stations (out of 554) had a p -value close to zero and many of the stations had a p -value close to one.

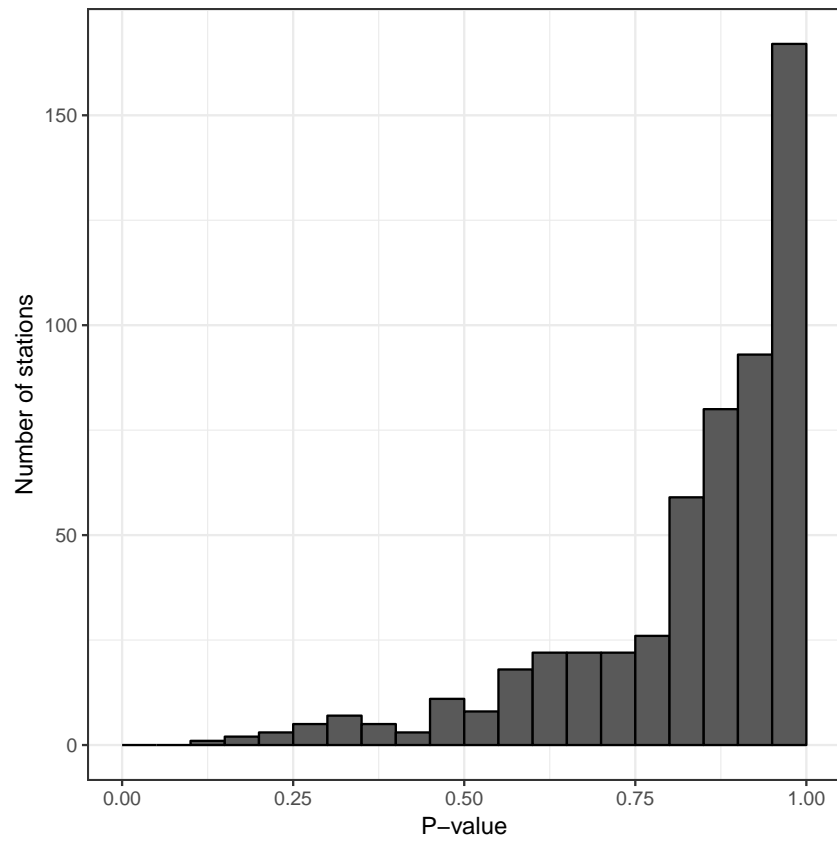


Figure 13: p -values of the Anderson-Darling test with null hypothesis stating that the data follow the GEV distribution.

3 Additional results

3.1 Convergence assessment

The MCMC simulation for the posterior inference for the full model (ψ , τ and ϕ modeled jointly) was evaluated by calculating the Gelman–Rubin statistic, and by investigating the trace plot and the autocorrelation plot of each parameter. Values of the Gelman–Rubin statistic and these plots are show below for a few selected parameters, namely, the parameters ψ_8 , τ_8 and ϕ_8 (all belonging station 8), the covariate coefficients $\beta_{\psi, \text{AREA}}$, $\beta_{\tau, \text{SAAR}}$ and $\beta_{\phi, \text{FPEXT}}$ and the hyperparameters $q_\psi = \sigma_{\epsilon\psi}^{-2}$, s_ψ and ρ_τ .

Table 1: Gelman-Rubin statistic for a subset of the parameters, namely, ψ_8 , $\beta_{\psi, \text{AREA}}$, q_ψ , τ_8 , $\beta_{\tau, \text{SAAR}}$, s_ψ , ϕ_8 , $\beta_{\phi, \text{FPEXT}}$, ρ_τ .

Parameter	Point est.	Upper C.I.
ψ_8	1.0000	1.0000
$\beta_{\psi, \text{AREA}}$	1.0001	1.0004
q_ψ	1.0005	1.0015
τ_8	0.9999	0.9999
$\beta_{\tau, \text{SAAR}}$	1.0009	1.0031
s_ψ	1.0069	1.0213
ϕ_8	1.0000	1.0000
$\beta_{\phi, \text{FPEXT}}$	1.0002	1.0007
ρ_τ	1.0117	1.0259

For the MCMC simulation, four chains of 10.000 samples with a burn-in of 2.000 samples were obtained. In this Section, only the 8.000 samples, that are left after removing the burn-in, are shown. Table 1 shows the Gelman–Rubin statistic, which is less than 1.1 for all the parameters tested, indicating adequate convergence for all MCMC chains. The trace plots in Figure 14 are all reasonable, i.e., there is no visual global trend, and the chains mix well. The plots in Figures 15, 16 and 17 show the autocorrelation of the MCMC simulation for each chain as a function of lag, one can see that the autocorrelation decreases rapidly as a function of lag for the covariate coefficients, $\beta_{\psi, \text{AREA}}$, $\beta_{\tau, \text{SAAR}}$ and $\beta_{\phi, \text{FPEXT}}$, and the parameters ψ_8 , τ_8 and ϕ_8 . The autocorrelation for the hyperparameters, q_ψ , s_ψ and ρ_τ also decreases as a function of lag but not as rapidly as the others parameters as expected. Results for other latent parameters are very similar to the results of the selected latent parameters. Likewise, results for other hyperparameters are very similar to the results of the selected hyperparameters.

3.2 Posterior estimates of parameters

Figures 18 and 19 show the hyperparameters that govern the spatial fields for ψ and τ , respectively. These parameters had joint prior densities $\pi(s_\psi, \rho_\psi)$ and $\pi(s_\tau, \rho_\tau)$, thus, the joint posterior densities of $(s_\psi, \rho_\psi)^\top$ and $(s_\tau, \rho_\tau)^\top$ along with the marginal densities of each parameter are shown in Figures 18 and 19. The posterior densities for the hyperparameters that govern the unstructured model errors, ϵ_ψ , ϵ_τ and ϵ_ϕ , namely, $\sigma_{\epsilon\psi}$, $\sigma_{\epsilon\tau}$ and $\sigma_{\epsilon\phi}$, are shown in Figure 20.

Table 2 shows the posterior mean, standard deviation and quantiles for the hyperparameters, $\sigma_{\epsilon\psi}$, s_ψ , ρ_ψ , $\sigma_{\epsilon\tau}$, s_τ , ρ_τ and $\sigma_{\epsilon\phi}$.

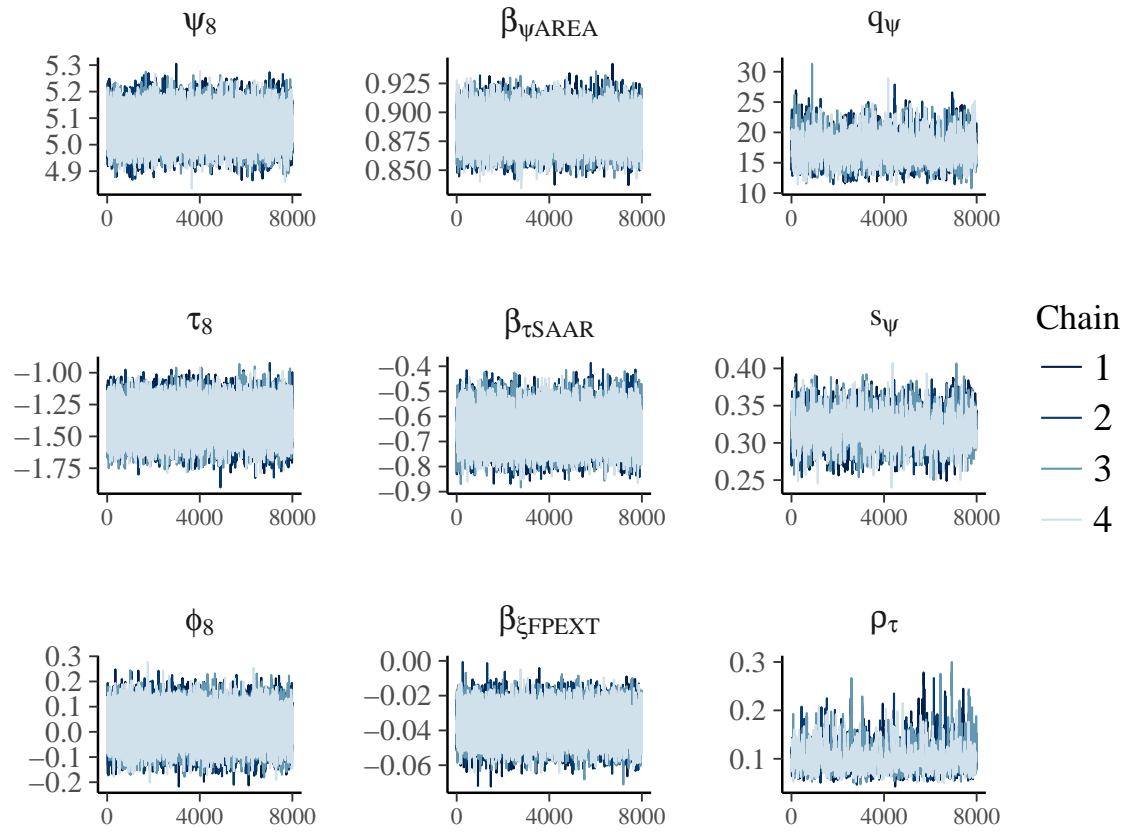


Figure 14: Trace plots for for a subset of the parameters, namely, ψ_8 , $\beta_{\psi, \text{AREA}}$, q_ψ , τ_8 , $\beta_{\tau, \text{SAAR}}$, s_ψ , ϕ_8 , $\beta_{\xi, \text{FPEXT}}$, ρ_τ .

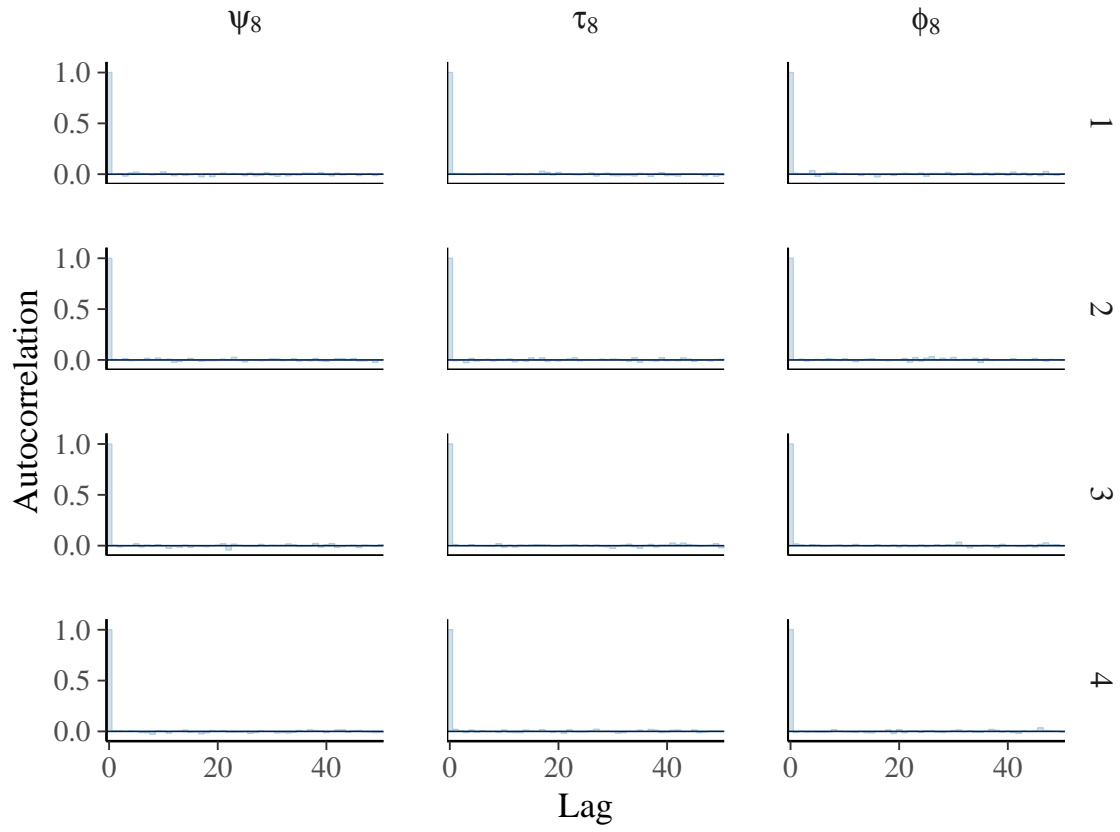


Figure 15: Autocorrelation plots for ψ_8 , τ_8 and ϕ_8 . The four horizontal panels represent each of the four chains.

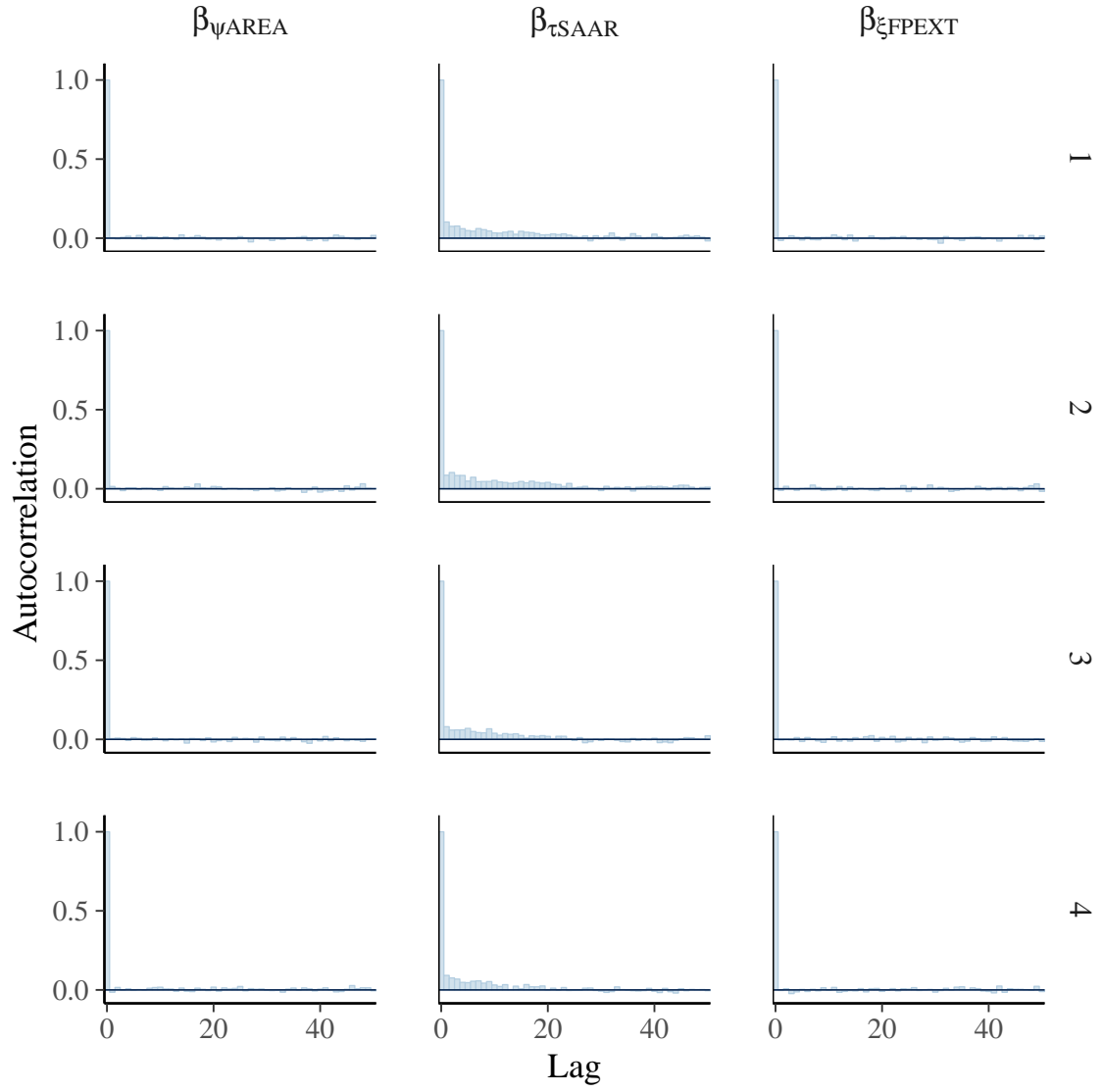


Figure 16: Autocorrelation plots for $\beta_{\psi,AREA}$, $\beta_{\tau,SAAR}$ and $\beta_{\phi,FPEXT}$. The four horizontal panels represent each of the four chains.

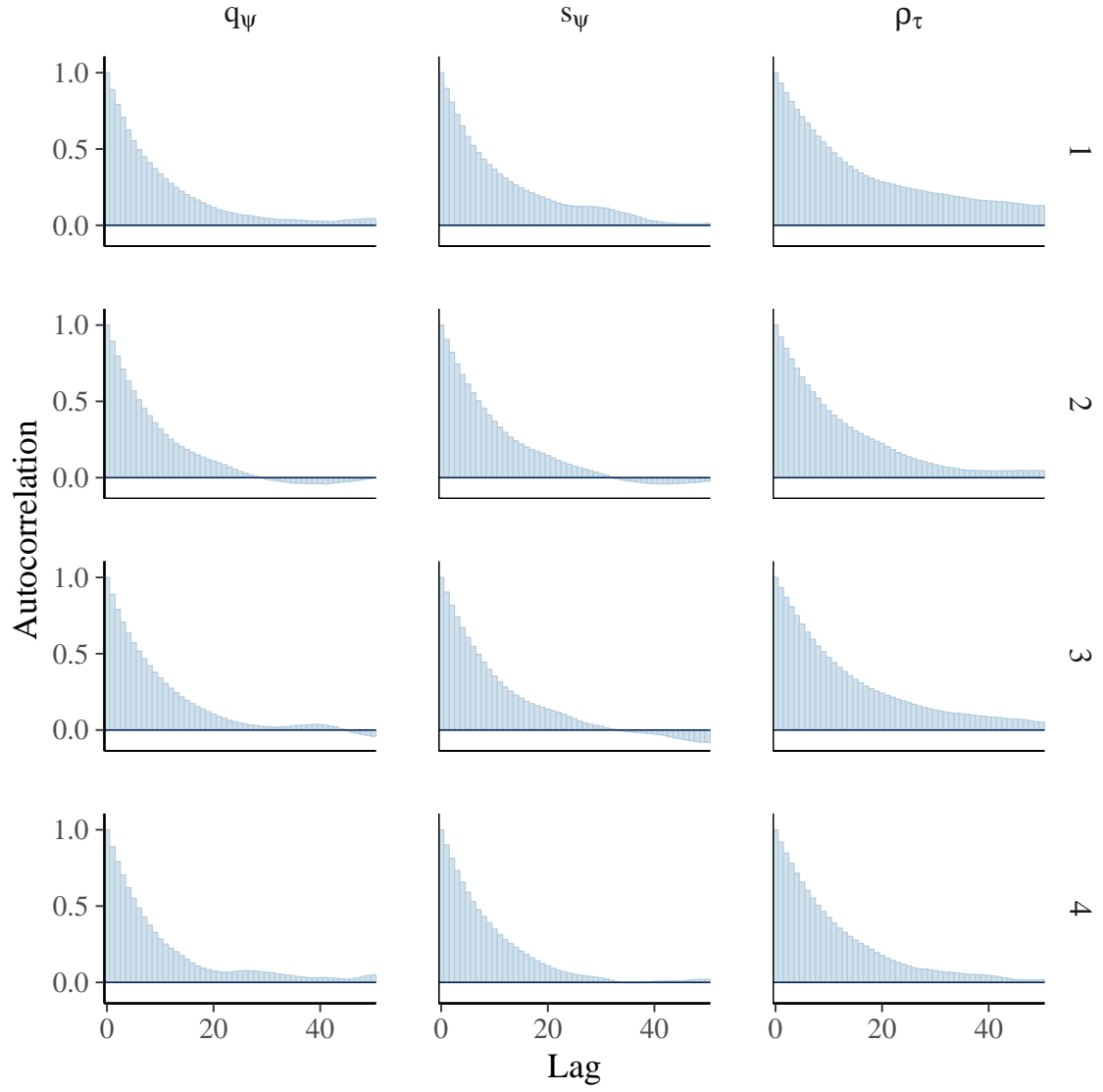


Figure 17: Autocorrelation plots for the hyperparameters q_ψ , s_ψ and ρ_τ . The four horizontal panels represent each of the four chains.

Table 2: Summary statistics for the posterior distribution of the hyperparameters.

Parameter	Mean	Sd.	Quantiles		
			2.5%	50%	97.5%
Hyperparameters for ψ					
$\sigma_{\epsilon\psi}$	0.241	0.016	0.211	0.241	0.273
s_ψ	0.319	0.023	0.275	0.318	0.364
ρ_ψ	0.053	0.008	0.040	0.052	0.071
Hyperparameters for τ					
$\sigma_{\epsilon\tau}$	0.128	0.011	0.106	0.128	0.149
s_τ	0.177	0.019	0.144	0.175	0.222
ρ_τ	0.102	0.027	0.062	0.098	0.166
Hyperparameters for ϕ					
$\sigma_{\epsilon\phi}$	0.066	0.006	0.053	0.065	0.079

Table 3 gives a summary of the posterior inference for the covariate coefficients for ψ , τ and ϕ . All the coefficients are well determined, i.e., their 95% posterior intervals do not contain zero.

Table 3: Summary statistics for the posterior distribution of the covariate coefficients for ψ , τ and ϕ .

Descriptor	Mean	Sd.	Quantiles		
			0.025	0.50	0.975
Covariate coefficients for ψ					
Intercept	-12.019	0.597	-13.189	-12.019	-10.831
log(AREA)	0.886	0.013	0.861	0.886	0.911
log(SAAR)	1.724	0.084	1.558	1.725	1.888
log(FARL)	3.705	0.314	3.093	3.705	4.324
BFIHOST ²	-3.228	0.135	-3.495	-3.228	-2.964
Covariate coefficients for τ					
Intercept	3.281	0.415	2.454	3.297	4.085
log(AREA)	-0.055	0.008	-0.071	-0.055	-0.039
log(SAAR)	-0.647	0.063	-0.767	-0.649	-0.522
log(FARL)	-1.108	0.193	-1.487	-1.108	-0.729
log(FPEXT)	-0.129	0.022	-0.172	-0.129	-0.087
log(URBEXT+1)	-0.661	0.219	-1.088	-0.663	-0.230
Covariate coefficients for ϕ					
Intercept	-0.102	0.024	-0.150	-0.102	-0.055
log(FPEXT)	-0.037	0.008	-0.053	-0.036	-0.021

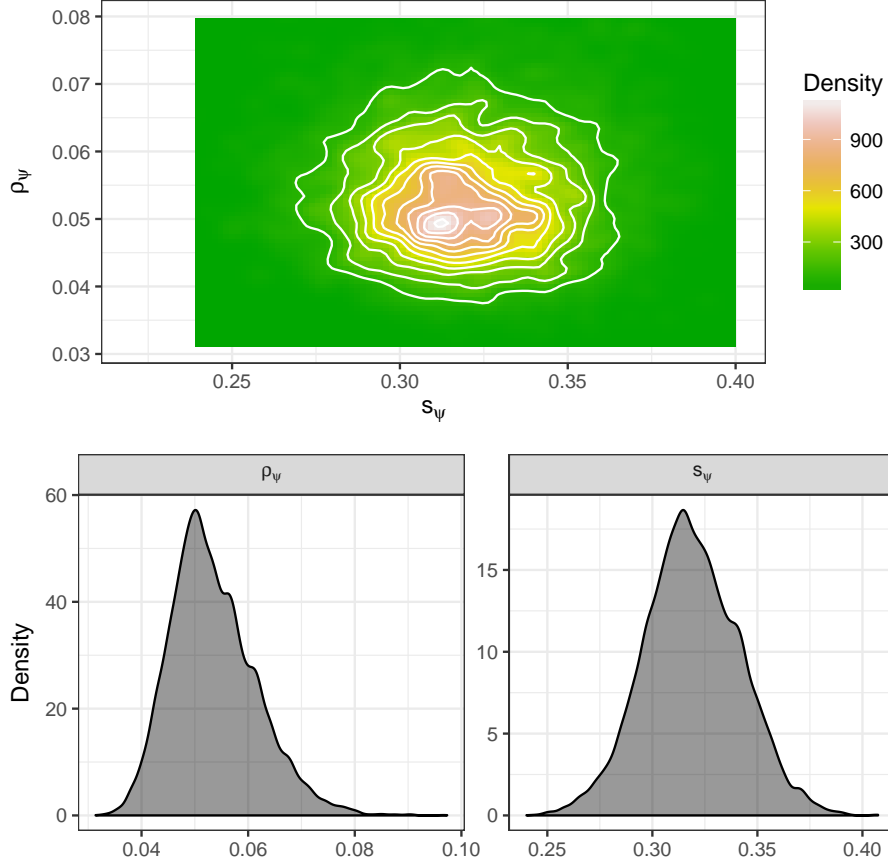


Figure 18: The joint posterior density of ρ_ψ and s_ψ , and the marginal posterior densities of ρ_ψ and s_ψ .

3.3 The effect of the spatial model components

The spatial components \mathbf{u}_ψ and \mathbf{u}_τ have a substantial effect on ψ and τ , respectively. Under the latent model, (5), the expected value of ψ_i and τ_i , for station, i , at a given location with covariates $\mathbf{x}_{\psi,i}$ and $\mathbf{x}_{\tau,i}$ is

$$\begin{aligned}\psi_i &= E(\psi_i | \boldsymbol{\beta}_\psi, \mathbf{u}_\psi) = \mathbf{x}_{\psi,i} \boldsymbol{\beta}_\psi + \mathbf{a}_i \mathbf{u}_\psi, \\ \tau_i &= E(\tau_i | \boldsymbol{\beta}_\tau, \mathbf{u}_\tau) = \mathbf{x}_{\tau,i} \boldsymbol{\beta}_\tau + \mathbf{a}_k \mathbf{u}_\tau.\end{aligned}\tag{8}$$

To quantify the effect of the spatial fields on μ_i and σ_i , one can imagine a scenario where two catchments have exactly the same covariates but have different locations. The expected value of $\exp(\psi_i)$ and $\exp(\tau_i)$ under the latent model are given by

$$\begin{aligned}E(\exp(\psi_i) | \boldsymbol{\beta}_\psi, \mathbf{u}_\psi) &= \exp(\mathbf{x}_{\psi,i} \boldsymbol{\beta}_\psi + \mathbf{a}_k \mathbf{u}_\psi + \sigma_{\epsilon_\psi}^2/2), \\ E(\exp(\tau_i) | \boldsymbol{\beta}_\tau, \mathbf{u}_\tau) &= \exp(\mathbf{x}_{\tau,i} \boldsymbol{\beta}_\tau + \mathbf{a}_k \mathbf{u}_\tau + \sigma_{\epsilon_\tau}^2/2).\end{aligned}\tag{9}$$

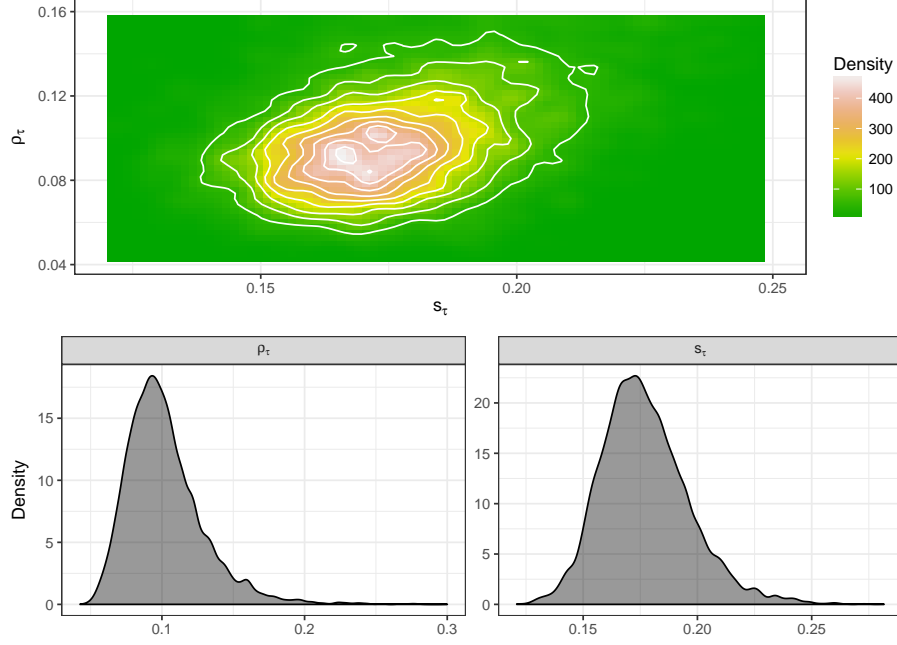


Figure 19: The joint posterior density of ρ_τ and s_τ , and the marginal posterior densities of ρ_τ and s_τ .

Using the expected values in Equation 9, the fact that $\mu_i = \exp(\psi_i)$ and $\sigma_i = \exp(\psi_i + \tau_i)$, and that ψ_i and τ_i are independent at the latent level, one can estimate the location and scale parameters of stations i and j as

$$E(\mu_i | \beta_\psi, \mathbf{u}_\psi) = \mu_i^* = \exp(\mathbf{x}_{\psi,i} \beta_\psi) \exp(\mathbf{a}_i \mathbf{u}_\psi) \exp(\sigma_{\epsilon\psi}^2/2),$$

$$E(\mu_j | \beta_\psi, \mathbf{u}_\psi) = \mu_j^* = \exp(\mathbf{x}_{\psi,j} \beta_\psi) \exp(\mathbf{a}_j \mathbf{u}_\psi) \exp(\sigma_{\epsilon\psi}^2/2),$$

$$E(\sigma_i | \beta_\psi, \mathbf{u}_\psi, \beta_\tau, \mathbf{u}_\tau) = \sigma_i^* = \exp(\mathbf{x}_{\psi,i} \beta_\psi + \mathbf{x}_{\tau,i} \beta_\tau) \exp(\mathbf{a}_i \mathbf{u}_\psi + \mathbf{a}_i \mathbf{u}_\tau) \exp(\sigma_{\epsilon\tau}^2/2 + \sigma_{\epsilon\psi}^2/2),$$

$$E(\sigma_j | \beta_\psi, \mathbf{u}_\psi, \beta_\tau, \mathbf{u}_\tau) = \sigma_j^* = \exp(\mathbf{x}_{\psi,j} \beta_\psi + \mathbf{x}_{\tau,j} \beta_\tau) \exp(\mathbf{a}_j \mathbf{u}_\psi + \mathbf{a}_j \mathbf{u}_\tau) \exp(\sigma_{\epsilon\tau}^2/2 + \sigma_{\epsilon\psi}^2/2).$$

Now if the same covariates are assumed for both stations then

$$\frac{\mu_j^*}{\mu_i^*} = \frac{\exp(\mathbf{x}_{\psi,j} \beta_\psi) \exp(\mathbf{a}_j \mathbf{u}_\psi) \exp(\sigma_{\epsilon\psi}^2/2)}{\exp(\mathbf{x}_{\psi,i} \beta_\psi) \exp(\mathbf{a}_i \mathbf{u}_\psi) \exp(\sigma_{\epsilon\psi}^2/2)} = \frac{\exp(\mathbf{a}_j \mathbf{u}_\psi)}{\exp(\mathbf{a}_i \mathbf{u}_\psi)},$$

$$\frac{\sigma_j^*}{\sigma_i^*} = \frac{\exp(\mathbf{x}_{\psi,j} \beta_\psi + \mathbf{x}_{\tau,j} \beta_\tau) \exp(\mathbf{a}_j \mathbf{u}_\psi + \mathbf{a}_j \mathbf{u}_\tau) \exp(\sigma_{\epsilon\tau}^2/2 + \sigma_{\epsilon\psi}^2/2)}{\exp(\mathbf{x}_{\psi,i} \beta_\psi + \mathbf{x}_{\tau,i} \beta_\tau) \exp(\mathbf{a}_i \mathbf{u}_\psi + \mathbf{a}_i \mathbf{u}_\tau) \exp(\sigma_{\epsilon\tau}^2/2 + \sigma_{\epsilon\psi}^2/2)} = \frac{\exp(\mathbf{a}_j \mathbf{u}_\psi + \mathbf{a}_j \mathbf{u}_\tau)}{\exp(\mathbf{a}_i \mathbf{u}_\psi + \mathbf{a}_i \mathbf{u}_\tau)}.$$

So, μ_j^* and σ_j^* can be written in terms of μ_i^* and σ_i^* as

$$\mu_j^* = \mu_i^* \frac{\mu_j^*}{\mu_i^*} = \mu_i^* \frac{\exp(\mathbf{a}_j \mathbf{u}_\psi)}{\exp(\mathbf{a}_i \mathbf{u}_\psi)},$$

$$\sigma_j^* = \sigma_i^* \frac{\sigma_j^*}{\sigma_i^*} = \sigma_i^* \frac{\exp(\mathbf{a}_j \mathbf{u}_\psi + \mathbf{a}_j \mathbf{u}_\tau)}{\exp(\mathbf{a}_i \mathbf{u}_\psi + \mathbf{a}_i \mathbf{u}_\tau)}.$$

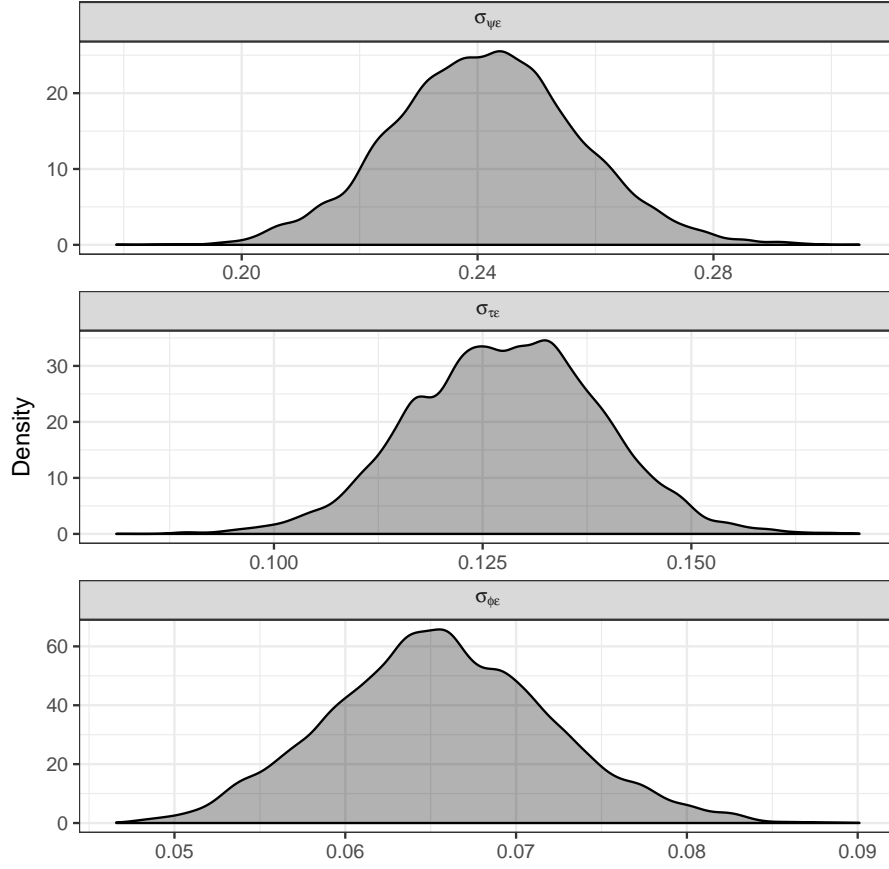


Figure 20: The marginal posterior density of $\sigma_{\epsilon\psi}$, $\sigma_{\epsilon\tau}$ and $\sigma_{\epsilon\phi}$.

3.4 The effect of the unstructured model components

Table 4 shows the effect of the unstructured model components on the location parameters, the scale parameters, the shape parameters, and the 100-year event of the GEV density.

Table 4: The effects of the unstructured model components on the location parameters, μ , the scale parameters, σ , the shape parameters, ξ , and the 100-year event (0.99 quantile) of the GEV density. To evaluate the effects of the unstructured model components the lower and upper quartiles of the standard normal distribution, ± 0.6745 , are used for comparison to the median, 0.0, and weighted with the posterior mean of the standard deviations $\sigma_{\epsilon\psi}$, $\sigma_{\epsilon\tau}$ and $\sigma_{\epsilon\phi}$, and transformed through the formulas for μ_i , σ_i , ξ_i and the 0.99 GEV quantile as functions of $\epsilon_{\psi,i}$, $\epsilon_{\tau,i}$ and $\epsilon_{\phi,i}$. So, then evaluating the effect of the unstructured model component $\epsilon_{\psi,i}$ on μ_i , for example, μ_i is computed with the median value of $\epsilon_{\psi,i}$, which is zero, and compared to $\epsilon_{\psi,i}$ equal to $\pm 0.6745\sigma_{\epsilon\psi}$ while keeping other covariates and random effects fixed. For μ and σ the effect is multiplicative, but for ξ the effect is (approximately) additive, and therefore the difference between predictions for the median and the quartiles was computed instead for ξ . Empty cells denote no effect.

Covariate	μ model		σ model		ξ model		100-year event	
	1st	3rd	1st	3rd	1st	3rd	1st	3rd
Unstr. ψ	0.850	1.177	0.850	1.177			0.850	1.177
Unstr. τ			0.917	1.090			0.948	1.056
Unstr. ϕ					-0.0436	0.0450	0.941	1.070

References

- J. Beirlant, Y. Goegebeur, J. Segers, J.L. Teugels, *Statistics of Extremes: Theory and Applications* (John Wiley & Sons, New York City, 2004)
- Ó.P. Geirsson, B. Hrafnkelsson, D. Simpson, Computationally efficient spatial modeling of annual maximum 24-h precipitation on a fine grid. *Environmetrics* **26**(5), 339–353 (2015). doi:10.1002/env.2343
- F. Lindgren, H. Rue, J. Lindström, An explicit link between Gaussian fields and Gaussian Markov random fields: the stochastic partial differential equation approach. *Journal of the Royal Statistical Society: Series B (Statistical Methodology)* **73**(4), 423–498 (2011). doi:10.1111/j.1467-9868.2011.00777.x
- E.S. Martins, J.R. Stedinger, Generalized maximum-likelihood generalized extreme-value quantile estimators for hydrologic data. *Water Resources Research* **36**(3), 737–744 (2000). doi:10.1029/1999WR900330
- R.L. Smith, Maximum likelihood estimation in a class of nonregular cases. *Biometrika* **72**(1), 67–90 (1985). doi:10.2307/2336336
- M.A. Stephens, Edf statistics for goodness of fit and some comparisons. *Journal of the American statistical Association* **69**(347), 730–737 (1974)
- T.L. Thorarinsdottir, K.H. Hellton, G.H. Steinbakk, L. Schlichting, K. Engeland, Bayesian regional food frequency analysis for large catchments. arXiv preprint 1802.09278 (2018)